

# Constraints on the reheating temperature from sizable tensor modes

Valerie Domcke<sup>a</sup> and Jan Heisig<sup>b</sup>

*a SISSA/INFN, 34126 Trieste, Italy*

*b RWTH Aachen University, 52056 Aachen, Germany*

## Abstract

Despite its importance for modeling the homogeneous hot early universe very little is experimentally known about the magnitude of the reheating temperature, leaving an uncertainty of remarkable 18 orders of magnitude. In this paper we consider a general class of polynomial inflaton potentials up to fourth order. Employing a Monte Carlo scan and imposing theoretical and experimental constraints we derive a robust lower limit on the energy scale at the end of inflation,  $V_{\text{end}}^{1/4} > 3 \times 10^{15}$  GeV for sizable tensor modes,  $r \geq 10^{-3}$ . If the reheating phase is perturbative and matter dominated, this translates into a lower bound on the reheating temperature, yielding  $T_{\text{rh}} > 3 \times 10^8$  ( $7 \times 10^2$ ) GeV for gravitational inflaton decay through a generic dimension five (six) operator.

# Contents

<b>1</b>	<b>Introduction</b>	<b>2</b>
<b>2</b>	<b>Analytic estimates of the energy scales <math>V_{\text{end}}</math> and <math>T_{\text{rh}}</math></b>	<b>4</b>
2.1	Constraining the energy density at the end of inflation . . . . .	5
2.2	Linking inflation to the reheating phase . . . . .	7
<b>3</b>	<b>Bounds for polynomial potentials</b>	<b>10</b>
3.1	Generic inflaton potentials for sizable tensor modes . . . . .	11
3.2	Constraints from Planck around $\Delta\phi = 0$ . . . . .	12
3.3	Constraints on $N_*$ . . . . .	14
3.4	Monte Carlo scan . . . . .	15
3.5	Properties of the inflaton potential . . . . .	17
<b>4</b>	<b>Results and discussion</b>	<b>19</b>
4.1	The energy density at the end of inflation . . . . .	19
4.2	A lower bound on the reheating temperature . . . . .	22
<b>5</b>	<b>Conclusion</b>	<b>25</b>
<b>A</b>	<b>CMB observables beyond leading order</b>	<b>27</b>
	<b>References</b>	<b>30</b>

## 1 Introduction

The primordial fluctuations of the cosmic microwave background (CMB) provide a unique window to energy scales far beyond the energies reached at colliders. With the recent Planck data [1], experiments have reached a remarkable sensitivity in decoding this information. The theoretical interpretation is necessarily prone to be model-dependent, with much progress in interpreting the recent data in terms of numerous specific inflation models, or classes of models, cf. Refs. [1–3] for a non-exhaustive list of examples. In this paper, we attempt to derive constraints on the relevant energy scales of the very early universe – in particular on the energy scale of the vacuum energy at the end of inflation and on the reheating temperature – in a more model-independent way, covering in particular all single-field inflationary models which can be approximated by a polynomial of degree four and a wide range of perturbative reheating scenarios.

The highest observable energy scale in the history of our universe is given by the potential energy driving inflation at the time when the largest scales observable today exited the horizon,

$$V_*^{1/4} = \left( \frac{3}{2} \pi^2 A_s \right)^{1/4} r^{1/4} M_{\text{P}} \simeq 3.3 \times 10^{16} \text{ GeV} r^{1/4}, \quad (1)$$

where  $A_s$  denotes the amplitude of the scalar perturbations generated during inflation and  $M_{\text{P}}$  is the reduced Planck mass,  $M_{\text{P}} = 2.43 \times 10^{18} \text{ GeV}$ . The unknown quantity is the tensor-to-scalar ratio  $r$  of the primordial fluctuations. Currently, the most stringent bounds on the tensor-to-scalar ratio  $r$  are obtained from a joint analysis of the BICEP2, Keck Array and Planck data, yielding  $r < 0.12$  [4]. Many large-field inflation models predict values of  $r$  close to this bound, and upcoming experiments will probe values of  $r$  in the percent region, cf. e.g. [5–7]. In this paper we focus on  $r \geq 10^{-3}$ , which might be probed in the near future.

During inflation the potential energy decreases as the inflaton field slowly rolls down its scalar potential until finally the potential energy density becomes a subdominant component of the total energy density. This is the onset of the reheating phase, which produces a thermal bath with some high temperature  $T_{\text{rh}}$  – the initial condition for the homogeneous hot early universe. The value of the reheating temperature is for example decisive for the question if thermal leptogenesis [8] can be responsible for the baryon asymmetry of our universe, which is only possible for  $T_{\text{rh}} \gtrsim 10^9 \text{ GeV}$  [9]. Moreover, the reheating temperature controls the relic abundances of long-lived particles such as gravitinos present in supergravity theories, which, depending on their mass, life-time and abundance, have the potential to explain dark matter [10, 11] or to cause serious problems [12–17] for the cosmological evolution of the universe, in particular endangering the success of big bang nucleosynthesis (BBN). Depending on the particle spectrum, a number of bounds have been derived on the reheating temperature [17–22]. For example, in the context of the 17-parameter  $R$ -parity conserving phenomenological minimal supersymmetric standard model, gravitino dark matter with a stau as next-to-lightest supersymmetric particle is viable for a reheating temperature of  $T_{\text{rh}} \lesssim 2 \times 10^9 \text{ GeV}$  [23] taking into account current collider bounds on the particle spectrum. However, despite its importance for modeling the very early universe, very little is experimentally known about the magnitude of the reheating temperature. It is bounded from below by the requirement of successful BBN and from above by the upper bound on the scale of inflation,  $10 \text{ MeV} < T_{\text{rh}} < 2 \times 10^{16} \text{ GeV}$ , leaving an uncertainty of remarkable 18 orders of magnitude.

With the unprecedented sensitivity of CMB measurements, a number of authors have recently revisited constraints on the energy scales of the early universe. In a data-driven approach, the scalar potential can be reconstructed around the pivot-scale of a given experiment [24, 25], cf. [1] for a recent analysis. This yields rather model-independent information

on the scalar potential, however only in the observable range, i.e. for a few Hubble times or correspondingly for a sub-planckian range of the inflaton field. Constraints on the reheating temperature have been derived for given inflation models by extracting constraints on the number of e-folds elapsed after the pivot-scale left the horizon from CMB measurements [26]. Since the total number of e-folds elapsed depends (weakly) on the reheating temperature, matching the temperature and Hubble horizon today implies bounds on the reheating temperature which can be as stringent as  $T_{\text{rh}} \gtrsim 10^8 - 10^{10}$  GeV [27], though highly dependent on the underlying inflation model as well as on the equation of state during reheating [28].

In this paper, we pursue a different approach, aiming to reduce in particular the dependence on the choice of the inflation model. Performing a dedicated Monte Carlo scan based on polynomial inflaton potentials up to degree four and taking into account the recent Planck constraints on the inflationary observables, we obtain a lower bound on the energy density at the end of inflation in the single-field slow-roll approximation,  $V_{\text{end}}^{1/4} > 3 \times 10^{15}$  GeV for  $r \geq 10^{-3}$  – remarkably close to the scale of grand unified theories (GUTs). If the reheating phase is matter dominated, this translates into a lower bound on the reheating temperature,  $T_{\text{rh}} > 3 \times 10^8$  ( $7 \times 10^2$ ) GeV for gravitational inflaton decay through a generic dimension five (six) operator. Both the bounds on  $V_{\text{end}}$  and  $T_{\text{rh}}$  are strengthened for larger values of  $r$ .

The remainder of this paper is organized as follows. In Sec. 2 we present analytical bounds on the energy density at the end of inflation and on the reheating temperature. These turn out to be highly dependent on the inflation model, motivating a systematic investigation of a broad class of models based on a Monte Carlo scan in Sec. 3. The results and discussion of this scan are presented in Sec. 4 before concluding in Sec. 5.

## 2 Analytic estimates of the energy scales $V_{\text{end}}$ and $T_{\text{rh}}$

Inflation is a well established concept to cure several short-comings of the standard model of cosmology, e.g. explaining the homogeneity and flatness of our universe on large scales [29]. Its predictions have been a striking success story, culminating in the measurement of the fluctuations of the CMB by the Planck satellite with remarkable precision, which strongly support the simplest model of single-field slow-roll inflation [1]. Here, the dynamics of inflation is governed by a scalar field  $\phi$  slowly moving down a scalar potential  $V(\phi)$ , the latter providing a large, nearly constant energy density necessary to exponentially inflate the universe,

$$3H\dot{\phi} = -V'(\phi), \quad (2)$$

with  $H$  denoting the Hubble parameter. Inflation ends at  $\phi_{\text{end}} = \phi(t_{\text{end}})$  when the kinetic energy of the inflaton  $\phi$  becomes comparable to the vacuum energy  $V_{\text{end}} = V(\phi_{\text{end}})$ . Observations of the CMB contain information about the scalar potential  $N_*$  Hubble times (e-folds)

earlier, when the pivot scale  $k_*^{-1}$  of a given experiment exited the horizon,

$$N_* = \int_{t_*}^{t_{\text{end}}} H dt \sim 50-60, \quad (3)$$

corresponding to a field value of  $\phi_* = \phi(t_*)$  and an energy scale  $V_* = V(\phi_*)$ .<sup>1</sup> One of the main open questions in inflationary model building is the nature of the scalar potential between  $\phi_*$  and  $\phi_{\text{end}}$ .

By measuring the properties of the primordial fluctuations in the CMB, in particular the amplitude  $A_s$  and the tensor-to-scalar ratio  $r$ , we can determine (or at least constrain)  $V_*$ , cf. Eq. (1). Can we use this information to constrain the energy scales at the end of inflation and reheating,  $V_{\text{end}}$  and  $T_{\text{rh}}$ ? After the pivot scale exited the horizon, inflation continued for a finite amount of time and the potential driving it cannot be arbitrary steep, so as not to violate slow-roll inflation. This will result in a lower bound on  $V_{\text{end}}$ , the value of the scalar potential at the end of inflation. This energy density is then converted into the energy density of the initial thermal bath. A crucial parameter is the time-scale of this transition, in the simplest setup governed by the decay rate of the massive inflaton particle after the end of inflation. Exploiting that the inflaton must at least interact gravitationally, the lower bound on  $V_{\text{end}}$  can be thus converted into a lower bound on the reheating temperature. In this section, our aim is to analytically examine the lower bound on  $V_{\text{end}}(r)$  which will then lead to a lower bound on the reheating temperature,  $T_{\text{rh}}(r)$ .

## 2.1 Constraining the energy density at the end of inflation

In this subsection we discuss analytical bounds on the drop of the potential energy during single-field slow-roll inflation. We discuss the most conservative case as well as the case of monomial potentials. These cases serve as reference cases for the later more general study presented in Secs. 3 and 4.

Let us take two points in the inflationary period 1 and 2,  $t_1 < t_2$ . Using the potential slow-roll parameters<sup>2</sup>

$$\epsilon = \frac{M_{\text{P}}^2}{2} \left( \frac{V'}{V} \right)^2, \quad \eta = M_{\text{P}}^2 \frac{V''}{V}, \quad (4)$$

we consider the ratio of the potentials at point 1 and 2,

$$\frac{V_1}{V_2} = \exp \left( \int_{V_2}^{V_1} \frac{dV}{V} \right) = \exp \left( \int_{\phi_2}^{\phi_1} \frac{\sqrt{2\epsilon}}{M_{\text{P}}} d\phi \right). \quad (5)$$

---

<sup>1</sup>More precisely, the CMB provides information on the shape of the scalar potential about 10 e-folds around this point.

<sup>2</sup>Effects of possible violation of the slow-roll approximation will be discussed when relevant.

In order to obtain a large value for  $V_1/V_2$  we require large  $\epsilon$  for as many e-folds,  $N$ , as possible. On the other hand, in order to allow for large  $N$ ,  $\epsilon$  has to stay below  $\epsilon_{\text{end}}$  (otherwise inflation ends). Hence, the largest  $V_1/V_2$  is obtained by a constant  $\epsilon$  just below  $\epsilon_{\text{end}}$  for as many e-folds as allowed. For this case the number of e-folds is obtained by

$$N = \int_{\phi_2}^{\phi_1} \frac{1}{\sqrt{2\epsilon} M_{\text{P}}} d\phi \geq \frac{\phi_1 - \phi_2}{\sqrt{2\epsilon_{\text{end}}} M_{\text{P}}}. \quad (6)$$

This determines the maximal field excursion allowed by slow-roll inflation. Hence, we can impose the conservative bound

$$\frac{V_1}{V_2} < e^{2\epsilon_{\text{end}} N}. \quad (7)$$

The corresponding potential yielding the largest  $V_1/V_2$  for a fixed number of e-folds has an exponential shape<sup>3</sup>

$$V(\phi) = V_1 e^{\sqrt{2\epsilon}(\phi_1 - \phi)/M_{\text{P}}}, \quad (8)$$

and fulfills the condition  $\eta = 2\epsilon$ . Note that in this case, some other mechanism is needed to end slow-inflation (e.g. a second scalar field as in hybrid inflation). Requiring  $\epsilon, \eta < 1$ , Eq. (7) yields an absolute lower bound of  $V_*/V_{\text{end}} < e^{N_*}$ , corresponding to a decrease of five orders of magnitude in the energy scale for  $N_* = 50$ . However, as  $\epsilon \sim 1/2$  is clearly excluded for the first 5-10 e-folds constrained by the CMB this bound is conservative and the dramatic exponential drop can at most take place for the last  $N'_*$  e-folds not constrained by the CMB.

Next, let us consider the situation where  $\eta(\phi) = q\epsilon(\phi)$ ,  $q \in \mathbb{R}$ . This corresponds to the case of a monomial potential  $V \propto \phi^p$ ,  $p > 0$  [31], and we can identify  $q = 2(p-1)/p$ . In this case

$$\frac{V_*}{V_{\text{end}}} = \left( \frac{\epsilon_{\text{end}}}{\epsilon_*} \right)^{p/2} = \left( \frac{4\epsilon_{\text{end}} N_* + p}{p} \right)^{p/2}. \quad (9)$$

Note that Eq. (9) contains the limiting case  $|\eta| \ll \epsilon$  for  $p \simeq 1$ . Conversely, if  $|\eta| \gg 2\epsilon$  we obtain  $V_*/V_{\text{end}} \rightarrow 1$ , since the potential must be extremely flat.

From this we can draw an important conclusion. In the special case of  $\eta = 2\epsilon = \text{constant}$ , the amplitude of the scalar potential during the last  $N'_* \sim 40$ -50 e-folds can indeed drop dramatically. However, this relies heavily on the specific exponential shape of the potential and is not the ‘generic’ case. Indeed for monomial potentials, Eq. (9) yields a much more restrictive bound of  $(V_*/V_{\text{end}})^{1/4} < 5.2$  for  $N_* < 60$  and  $p < 3$ , whereby  $p \geq 3$  is already strongly disfavored by the recent Planck data [1]. In Sec. 3 we will hence pursue the ansatz of a fourth order polynomial in order to systematically study the largest  $V_*/V_{\text{end}}$  that additionally are in agreement with current observations from the CMB. In this ansatz it is impossible to achieve a constant value of  $\eta = 2\epsilon$  for all values of  $\phi$  for non-vanishing  $\epsilon$ .<sup>4</sup> In Sec. 4 we will

<sup>3</sup>Models with an exponential inflaton potential were discussed e.g. in [30].

<sup>4</sup>To maintain a constant value of  $\eta = 2\epsilon$  and hence saturate the bound Eq. (7) for  $N_* \simeq 50$  e-folds a polynomial of order  $\sim 180$  is needed.

find that within this framework  $V_*/V_{\text{end}}$  is significantly smaller than the bound (7), namely  $V_*/V_{\text{end}} \lesssim 10 - 1000$ , depending on the value of the tensor-to-scalar ratio  $r$ . Moreover we will investigate the fine-tuning required in the parameters of the potential in order to saturate this bound.

Before concluding this section, let us add a brief comment on the slow-roll approximation used in this section. To obtain large values of  $V_*/V_{\text{end}}$  we are interested in fairly steep potentials. In particular we will consider potentials which are well described by the slow-roll limit close to  $\phi_*$  (as dictated by the Planck data) but may have sizable corrections as  $\epsilon \sim 1$  is approached towards the end of inflation. In other words, the violation of the slow-roll limit is typically accompanied by an accelerating inflaton field. Considering the full equation of motion for the inflaton,

$$\ddot{\phi} + 3H\dot{\phi} = -V'(\phi), \quad (10)$$

we note that for monotonic potentials and an accelerating inflaton field, the slow-roll approximation over-estimates the velocity  $|\dot{\phi}|$  and hence the distance in field space  $|\phi_* - \phi_{\text{end}}|$ . This effect is however typically (over)compensated since for an accelerating inflaton field, the slow-roll approximation under-estimates the value of  $|\phi_* - \phi_{\text{end}}|$  when inflation ends, cf. footnote 6. In general, the effect is however expected to be small since it only concerns the very end of inflation. We will return to this point in Sec. 4.2.

## 2.2 Linking inflation to the reheating phase

Inflation is followed by a phase of reheating, during which the vacuum energy is converted into a hot thermal bath of standard model particles [32]. In the simplest setup, this implies an intermediate stage governed by the coherent oscillations of a heavy scalar field, which then decays into the standard model fields with a total decay rate  $\Gamma_\phi$  [33–35]. This field can but must not be the inflaton field itself.

A scalar field oscillating in a potential  $V(\phi) = a\phi^p$  implies an equation of state [36]

$$\omega = \frac{\langle p_\phi \rangle}{\langle \rho_\phi \rangle} = \frac{p-2}{p+2}, \quad (11)$$

where the energy density  $\rho_\phi = \dot{\phi}^2/2 + V(\phi)$  and the pressure  $p_\phi = \dot{\phi}^2 - V(\phi)$  are related through the virial theorem,  $p \langle V(\phi) \rangle = 2 \langle \dot{\phi}^2/2 \rangle$ . Here we have assumed the oscillation frequency  $\dot{\phi}/\phi$  to be much larger than the expansion rate  $H$ , as is the case very soon after the end of inflation. Let us first assume for simplicity that the end of inflation is followed immediately by a matter dominated phase with  $\omega = 0$ . In other words, we take the potential for the scalar field to be essentially quadratic:

$$V(\phi) = \frac{1}{2}m_\phi^2(\phi + c)^2 \quad \text{for } \phi \leq \phi_{\text{end}} \quad \text{with } V(\phi_{\text{end}}) = V_{\text{end}}, \quad (12)$$

thus matching the energy densities at the end of inflation and at the onset of reheating.<sup>5</sup> Finally imposing that inflation is indeed over at  $\phi_{\text{end}}$ ,<sup>6</sup>

$$\epsilon(\phi) \geq \epsilon_{\text{end}} \quad \text{for } \phi \leq \phi_{\text{end}} \quad (13)$$

we find that the mass of the scalar field is bounded from below,

$$m_\phi^2 \geq \epsilon_{\text{end}} V_{\text{end}} / M_{\text{P}}^2. \quad (14)$$

If indeed the inflaton field itself is responsible for reheating and the transition from inflation to reheating is perturbative, we can match not only the amplitude of the potential at  $\phi_{\text{end}}$  but also the first derivative. In this case the bound in Eq. (14) becomes an equality.

For completeness, let us consider also the case that the transition from inflation to a matter dominated phase is not instantaneous. For example, picture the more general situation that the potential for the scalar field  $\phi$  is given by

$$V(\phi) = \frac{1}{2} m_\phi^2 \phi^2 \left( 1 + b \frac{|\phi|^{p-2}}{M_{\text{P}}^{p-2}} \right), \quad (15)$$

for  $p > 2$  where for simplicity we have chosen the origin of field-space so as  $V(0) = 0 = V'(0)$ . This corresponds to the situation where just after the end of inflation, while the inflaton oscillation is large, the potential is governed by some higher order polynomial  $\phi^p$  until towards the end of reheating, as  $\phi \ll M_{\text{P}}$ , the quadratic term comes to dominate. According to Eq. (11), this models an equation of state with  $\omega$  in the interval  $\{0, 1\}$ , in particular including the equation of state of radiation,  $\omega = 1/3$ , corresponding to a quartic potential. We do not consider  $0 \leq p < 2$  since the linear and constant terms in the scalar potential are always absorbed by our definition of the origin of field space. Fractional exponents in this range lead to potentials which are not differentiable at their minimum.

Matching to  $V(\phi_{\text{end}}) = V_{\text{end}}$  and  $\epsilon(\phi_{\text{end}}) \geq \epsilon_{\text{end}}$  as above yields

$$m_\phi^2 \gtrsim \frac{2V_{\text{end}}}{bM_{\text{P}}^2} \left( \frac{2\epsilon_{\text{end}}}{p^2} \right)^{\frac{p}{2}}, \quad (16)$$

---

<sup>5</sup>Here, we are not specifying the details of the reheating mechanism. In particular, this may hold also for scenarios which involve tachyonic preheating [37]. In this case the large majority of the vacuum energy density is rapidly converted into low-momentum modes of a symmetry breaking field which again implies an equation of state with  $\omega = 0$  if the symmetry breaking field is sufficiently heavy.

<sup>6</sup>Note that more precisely, the end of inflation is reached when the first Hubble slow-roll parameter  $\epsilon_H = \dot{\phi}^2 / (2H^2)$  reaches  $\epsilon_H = 1$  [38]. As long as slow-roll is a good approximation,  $\epsilon_H \simeq \epsilon$ . At the end of inflation, when slow-roll is violated,  $\epsilon_H \geq 1$ , one finds for an accelerating inflaton field  $\epsilon(\phi) > 1$ , allowing us to set  $\epsilon_{\text{end}} = 1$  in Eq. (13). In the (untypical) case of a decelerating inflaton field at the end of inflation, this only holds approximately.



where we have assumed that the  $\phi^p$  term dominates in the initial reheating stage (else it is irrelevant and Eq. (14) applies). We immediately see that for  $b \sim 1$ , i.e. if the quadratic and  $\phi^p$  term become comparable at  $\phi \sim M_{\text{P}}$  then Eq. (16) yields a comparable bound to Eq. (14). In particular for  $p = 3$  ( $p = 4$ ) the bound on  $m_\phi$  is weakened by merely a factor of about 2 (6). If  $b \gg 1$ , then the bound on  $m_\phi$  disappears. This corresponds to the limiting case of a pure  $\phi^p$  potential. For  $b < 1$ , Eq. (16) seems to improve on the bound of Eq. (14), note however that in the derivation of Eq. (16) we have assumed the  $\phi^p$  term to be dominant, i.e.  $b$  is bounded from below. We conclude that as long as the quadratic term is not strongly suppressed compared to higher order terms in the reheating potential, the bound in Eq. (14) is not significantly weakened. The following results are hence not very sensitive to the assumption of a purely quadratic reheating potential, or correspondingly to the assumption of  $\omega = 0$ . For concreteness, we will however focus on  $\omega = 0$  in the following.

The reheating temperature is defined as the temperature of the thermal bath when half of the total energy density has been converted into radiation. This happens when the decay rate of the massive  $\phi$ -particle becomes comparable to the Hubble rate,  $H \simeq \Gamma_\phi$ . Exploiting the expression for the energy density  $\rho_r$  of a thermal bath at temperature  $T$  as well as the Friedmann equation,

$$\rho_r = \frac{\pi^2}{30} g_* T^4, \quad \rho_{\text{tot}} = 3H^2 M_{\text{P}}^2, \quad (17)$$

where  $g_*$  denotes the effective number of massless degrees of freedom in the thermal bath ( $g_*^{\text{rh}} = 427/4$  for the standard model at high energies), this yields<sup>7</sup>

$$T_{\text{rh}} = \left( \frac{45}{\pi^2 g_*^{\text{rh}}} \right)^{1/4} \sqrt{\Gamma_\phi M_{\text{P}}}. \quad (18)$$

A lower bound on this temperature can be obtained by assuming only gravitational interactions for the inflaton, resulting in the following effective dimension five operators:

$$\lambda \frac{m_\phi^2}{M_{\text{P}}} \phi B^* B, \quad \lambda \frac{m_\phi}{M_{\text{P}}} \phi \bar{f} f, \quad (19)$$

where  $B$  and  $f$  are bosonic and fermionic fields, respectively, and  $\lambda$  is a dimensionless coupling. Such operators may be sourced by a coupling of the inflaton field to the kinetic terms of the respective particles.<sup>8</sup> The decay rate of the non-relativistic particle  $\phi$  into a pair of light

---

<sup>7</sup>Here, we use  $H = \Gamma_\phi$  and  $\rho_r = \rho_{\text{tot}}/2$  at  $T = T_{\text{rh}}$ . Corrections arise due to the relativistic time delay in the decay of the  $\phi$ -particle and from the precise factor  $\alpha$  in  $\rho_r = \alpha \rho_{\text{tot}}|_{H=\Gamma_\phi}$ , which has to be determined numerically. However, even taking into account these effects, Eq. (17) typically remains a good estimate for the reheating temperature, cf. e.g. Ref. [39].

<sup>8</sup>In the context of supergravity, such effective operators for the decay into a supermultiplet  $X$  are generated e.g. by a term  $\lambda M_{\text{P}}^{-1} \phi |X|^2$  in the Kähler potential, which leads e.g. to a term  $\lambda M_{\text{P}}^{-1} \phi \partial_\mu X^* \partial^\mu X$  for the corresponding scalar field in the effective Lagrangian, see also [40]. However, determining the dominant

bosons or fermions is given by

$$\Gamma_\phi \sim \frac{\lambda^2 m_\phi^3}{16\pi M_{\text{P}}^2}. \quad (20)$$

In the case of multiple decay modes Eq. (20) turns into the sum over the respective partial widths. One might also imagine the situation in which dimension-5 operators are forbidden or strongly suppressed. In this case there are additional suppression factors of  $m_\phi/M_{\text{P}}$  with respect to Eq. (19). In summary, this yields

$$\begin{aligned} T_{\text{rh}}^{\text{dim } 5} &\sim \left(\frac{45}{\pi^2 g_*^{\text{rh}}}\right)^{1/4} \sqrt{\frac{\lambda^2 m_\phi^3}{16\pi M_{\text{P}}}}, \\ T_{\text{rh}}^{\text{dim } 6} &\sim \left(\frac{45}{\pi^2 g_*^{\text{rh}}}\right)^{1/4} \sqrt{\frac{\lambda^2 m_\phi^5}{16\pi M_{\text{P}}^3}}. \end{aligned} \quad (21)$$

Plugging Eqs. (1), (7), (14) and (21), this yields (for the case of the dimension five operator)

$$T_{\text{rh}}^{\text{dim } 5} \gtrsim 3.7 \text{ MeV } \lambda \left(\frac{A_s}{2.2 \times 10^{-9}}\right)^{3/4} \left(\frac{r}{0.1}\right)^{3/4} \left(\frac{\epsilon_{\text{end}}}{1/2}\right)^{3/4} \left(\frac{427/4}{g_*^{\text{rh}}}\right)^{1/4} e^{-3/2(N'_* \epsilon_{\text{end}} - 20)}, \quad (22)$$

for the exponential potential and correspondingly with Eq. (9) for the monomial potentials

$$T_{\text{rh}}^{\text{dim } 5} \gtrsim 6.0 \times 10^9 \text{ GeV } \lambda \left(\frac{A_s}{2.2 \times 10^{-9}}\right)^{3/4} \left(\frac{r}{0.1}\right)^{3/4} \left(\frac{427/4}{g_*^{\text{rh}}}\right)^{1/4} \left(\frac{\epsilon_{\text{end}}}{1}\right)^{3/4} \frac{f(r, N_*, \epsilon_{\text{end}})}{0.09}, \quad (23)$$

where  $f(r, N_*, \epsilon_{\text{end}}) = (r/(16\epsilon_{\text{end}}))^{3rN_*\epsilon_{\text{end}}/(32\epsilon_{\text{end}}-2r)}$  (for typical values  $f(0.1, 50, 1) \simeq 0.09$ ). Eq. (23) leads to  $T_{\text{rh}} \gtrsim 10^9 \text{ GeV}$  for  $0.001 < r < 0.1$  and  $\lambda \simeq 1$  with a very mild dependence on the choice of  $\epsilon_{\text{end}}$  and  $N_*$ . On the contrary, in Eq. (22) these parameters enter in the exponent, implying that for  $N'_* \epsilon_{\text{end}} \gtrsim 20$  the bound does not impose any restrictions beyond the requirement that thermalization of the universe has to take place well before BBN,  $T_{\text{rh}} > 10 \text{ MeV}$ . The huge difference between Eq. (22) and Eq. (23) stresses the need for a more model-independent approach, which we will address in the next section.

Finally, we mention that other mechanisms can prolong the reheating phase by delaying the thermalization of the universe due to kinematic effects (such as e.g. kinematic blocking). These effects can further weaken the bound on  $T_{\text{rh}}$  but are highly model-dependent [41, 42].

### 3 Bounds for polynomial potentials

The previous section served to obtain an analytical estimate for a lower bound on the reheating temperature. In a next step, we will back this up by performing a systematic Monte Carlo scan 

---

 contribution to the decay of the inflaton depends upon the SUSY breaking scale and the details of the super-symmetric particle spectrum.

of suitable inflationary potentials. We will specify the class of scalar potentials in Sec. 3.1. Secs. 3.2 and 3.3 are dedicated to the imposed constraints. The procedure of the scan will be detailed in Sec. 3.4 while in Sec. 3.5 we will discuss the properties of the inflationary potentials particularly interesting for exploring the lower bound on the reheating temperature. Our results are then presented in Sec. 4.

### 3.1 Generic inflaton potentials for sizable tensor modes

Our aim in this section is to systematically sample a broad range of inflation models. We restrict ourselves to single-field slow-roll inflation models, implying that the potential must allow for approximately 50-60 e-folds of inflation and must allow for inflation to end, i.e.  $\epsilon(\phi_{\text{end}}) \sim 1$ . This in particular excludes situations in which the inflaton field becomes trapped in a false vacuum which it can only leave by tunneling through a potential barrier or if it is assisted by the dynamics of a further field. Instead, we require the potential to be sufficiently ‘well-behaved’, i.e. to support a small but strictly monotonous slope over a sufficiently large field range. In this spirit, we expand the potential around the Planck pivot scale  $\phi_*$ , where it is well constrained by the CMB data, but truncate the expansion at fourth order:

$$V(\Delta\phi) \simeq V_* \left( 1 + \sum_{n=1}^4 c_n \left( \frac{\Delta\phi}{M_{\text{P}}} \right)^n \right), \quad c_n = \frac{M_{\text{P}}^n}{V_* n!} \left. \frac{\partial^n V}{\partial \phi^n} \right|_{\phi_*}, \quad (24)$$

with  $\Delta\phi = \phi - \phi_*$ . The effect of the truncation is of course independent of the choice of  $\phi_*$ , e.g. all potentials of the type

$$V(\phi) = \sum_{n=0}^4 a_n \phi^n \quad (25)$$

are trivially included in the ansatz (24), including the monomial potentials with integer exponent  $p \leq 4$ . The motivation for this truncation (apart from the obvious effect of practicability) is manifold. For small-field inflation models,  $\Delta\phi \ll M_{\text{P}}$ , the Taylor expansion of any  $V(\phi)$  around  $\phi_*$  quickly converges and Eq. (24) is a good approximation to the full potential. For large-field inflation models, which we are more interested in for the purpose of this paper since they come with a high scale of inflation, higher-order operators with sizable coefficients will make a sufficiently long period of slow-roll inflation difficult, unless these coefficients are very carefully tuned to ensure a cancellation of these contributions. Viable large-field models of inflation hence typically forbid these terms, e.g. by taking the inflaton to be a pseudo Nambu-Goldstone boson as in natural inflation [43, 44] or, in supersymmetric models, by employing a shift-symmetric Kähler potential which is only broken by a renormalizable superpotential [45]. Our ansatz (24) thus covers a large range of known inflation models (cf. Ref. [1] for a recent overview in light of recent experimental results): Monomial potentials with non-integer power

$p$  are well approximated by a polynomial of degree four, the crucial quantity  $V_*/V_{\text{end}}$  differs by at most a factor of about 0.6-1.5 between the pure monomial and its approximation. It moreover trivially contains quadratic and quartic hilltop inflation [46], cf. Eq. (25), and approximately contains natural inflation, considering  $\cos(\phi/f)$  (with  $\phi \ll f$ ) truncated at fourth order. In a broader sense, it covers all renormalizable models of inflation. Finally note that typical small- $r$  inflation models such hybrid inflation models [47,48]<sup>9</sup> (putting aside the requirement of reaching  $\epsilon(\phi_{\text{end}}) \sim 1$ ) and Starobinsky-type inflation models [50] (including the original  $R^2$  model as well recent rediscoveries of this exponentially flat potential [51–55]) typically feature a very small  $V_*/V_{\text{end}} \lesssim 10$  and are hence not of particular interest for the lower bound on  $V_{\text{end}}$  and  $T_{\text{rh}}$ .

Based on Eq. (24), we will systematically search for suitable inflation potentials by means of a Monte Carlo scan, restricting the coefficients of Eq. (24) by the CMB observations and constraining the number of e-folds of inflation  $N_*$  by comparing the CMB pivot scale with the present Hubble horizon. We take the inflaton to be rolling towards the origin in field-space, i.e.  $\Delta\phi < 0$ , and consider the range starting from  $\Delta\phi = 0$  and ending with  $\epsilon(\Delta\phi_{\text{end}}) \sim 1$ .

### 3.2 Constraints from Planck around $\Delta\phi = 0$

We consider the CMB observables  $A_s, n_s, \alpha_s, \kappa_s, r$  which can be expressed in terms of the potential slow-roll parameters  $\epsilon, \eta$  and

$$\xi^2 = M_{\text{P}}^4 \frac{V'V^{(3)}}{V^2}, \quad \sigma^3 = M_{\text{P}}^6 \frac{V'^2V^{(4)}}{V^3}, \quad (26)$$

to leading order by

$$\begin{aligned} A_s &= \frac{V}{24\pi^2\epsilon M_{\text{P}}^4} [1 + \mathcal{O}(\epsilon)], \\ n_s &= 1 - 6\epsilon + 2\eta + \mathcal{O}(\epsilon^2), \\ \alpha_s &= 16\epsilon\eta - 24\epsilon^2 - 2\xi^2 + \mathcal{O}(\epsilon^3), \\ \kappa_s &= -192\epsilon^3 + 192\epsilon^2\eta - 32\epsilon\eta^2 - 24\epsilon\xi^2 + 2\eta\xi^2 + 2\sigma^3 + \mathcal{O}(\epsilon^4), \\ r &= 16\epsilon + \mathcal{O}(\epsilon^2), \end{aligned} \quad (27)$$

where the slow-roll parameters are understood to be evaluated at  $\Delta\phi = 0$ . For the computations in our scan we use, however, expressions for the CMB observables beyond leading order which are given in the Appendix. We checked that in our scan the slow-roll parameters

$$\epsilon = \frac{1}{2}c_1^2, \quad \eta = 2c_2, \quad \sqrt{\xi^2} = \sqrt{6c_1c_3}, \quad \sqrt[3]{\sigma^3} = \sqrt[3]{24c_1^2c_4} \quad (28)$$

---

<sup>9</sup>These are listed under the name spontaneously broken supersymmetric models in [1]. Even a variant of the minimal hybrid inflation model constructed to achieve a large tensor-to-scalar ratio within an intermediate field excursion  $\Delta\phi_{\text{end}} \lesssim M_{\text{P}}$  only yields  $V_*/V_{\text{end}} \lesssim 1.05$  [49].

are indeed sufficiently small compared to one in order to ensure the validity of the expansion (see e.g. [38]). This is in particular the case for potentials that allow for a sufficiently long period of inflation  $N_* \gtrsim 50$  and values of the potential drop of interest to our work,  $V_*/V_{\text{end}} \gtrsim 10$ , where the absolute values of the above parameters are found to be well below 0.1.

The Planck collaboration has provided stringent constraints on these observables, which we take into account by calculating the  $\chi^2$  of each parameter point  $\mathbf{v} = (\ln A_s, n_s, r, \alpha_s)^T$ ,

$$\chi^2(A_s, n_s, r, \alpha_s) = (\mathbf{v} - \bar{\mathbf{v}})^T \mathcal{C}^{-1} (\mathbf{v} - \bar{\mathbf{v}}). \quad (29)$$

Here  $\bar{\mathbf{v}}$  contains the mean values of the  $1\sigma$  confidence intervals measured by Planck,<sup>10</sup>

$$\begin{aligned} \ln(10^{10} A_s) &= 3.104 \pm 0.035, & n_s &= 0.9644 \pm 0.0049, \\ r &= 0 \pm 0.069, & \alpha_s &= -0.0085 \pm 0.0076, & \kappa_s &= 0.025 \pm 0.013, \end{aligned} \quad (30)$$

and  $\mathcal{C}$  is the corresponding covariance matrix,  $\mathcal{C} = \boldsymbol{\sigma}^T X \boldsymbol{\sigma}$ . Here  $\boldsymbol{\sigma}$  is a vector containing the  $1\sigma$  uncertainties of the observables in Eq. (30) and the correlation matrix  $X$  encodes the correlations between the observables. Note that here we assume that  $\Delta\phi = 0$  corresponds to the Planck pivot scale, a constraint we will explicitly impose in the next section. We use the data from the Planck legacy arxiv for the base-model including a non-vanishing running and tensor-to-scalar ratio, including the high multipole joint TT, TE and EE constraints and the low multipole polarization constraints [56]. This corresponds to confidence intervals given in the last column of Tab. 4 in the recent Planck analysis [1]. By reproducing the marginalized joint 68% and 95% C.L. constraints in the  $n_s$ - $\alpha_s$ - and  $n_s$ - $r$ - plane in [1, 57] we checked that the Gaussian approximation provides a good description of the uncertainties. At the time of writing, the Planck collaboration had not released an analysis based on a model including a non-vanishing  $r$ ,  $\alpha_s$  and  $\kappa_s$ . We thus base our analysis on the data provided for the ( $r \neq 0$ ,  $\alpha_s \neq 0$ ,  $\kappa_s = 0$ ) model. A priori, this could be a serious limitation since fairly strong correlations between these parameters have been pointed out, e.g. the  $\alpha_s$ - $\kappa_s$  correlation was found to be important in [58]. However, performing the Monte Carlo scan detailed in Sec. 3.4, we find that the requirement of sustaining inflation for a suitable period (roughly 50 - 65 e-folds, see Sec. 3.3 for details) enforces  $-2 \times 10^{-3} < \kappa_s < 10^{-4}$ , independently of the much weaker bound in Eq. (30), cf. left panel of Fig. 1. This justifies the use of Eq. (29), i.e. taking into account the correlations between  $A_s, n_s, \alpha_s$  and  $r$  but varying  $\kappa_s$  independently. In the following figures, we show the resulting 95% confidence region, corresponding to  $\chi^2 < 9.72$ .

---

<sup>10</sup>Of course the physical meaning of  $r$  as the tensor-to-scalar ratio implies  $r > 0$  and we will consider only parameter points with  $r > 0$ .

### 3.3 Constraints on $N_*$

In the previous section we have focused on how the Planck data constrains the scalar potential locally, i.e. around  $\Delta\phi = 0$ . Furthermore, the scalar potential must fulfill an important global property, it must sustain a suitable amount of inflation between  $\Delta\phi = 0$  and  $\Delta\phi_{\text{end}}$ . This is ensured by comparing the CMB pivot scale  $k_*^{-1}$  with today's Hubble horizon. With the expansion history of the universe from reheating until today described by the standard model of cosmology, this determines the number of e-folds  $N_*$  of inflation elapsed after the scale  $k_*^{-1}$  exited the horizon:  $N_* = \ln(a_0/a_*) + \ln(a_{\text{end}}/a_0)$ . Tracking the expansion history of the universe epoch by epoch, this yields [26, 59]:

$$N_*^{\text{cond}} \simeq 66.64 - \ln\left(\frac{k_*}{a_0 H_0}\right) + \frac{1}{4} \ln\left(\frac{V_*}{M_{\text{P}}^4}\right) + \frac{1}{4} \ln\left(\frac{V_*}{V_{\text{end}}}\right) + \frac{1-3\omega}{12(1+\omega)} \ln\left(\frac{\rho_{\text{rh}}}{V_{\text{end}}}\right), \quad (31)$$

where  $\omega$  denotes the equation of state during reheating,  $\rho_{\text{rh}}$  is the energy density related to the reheating temperature and  $k_* = a_* H_* = 0.002 \text{ Mpc}^{-1}$  is the Planck pivot scale.  $a_0$  and  $H_0$  are the scale factor and Hubble constant today, where we work in units with  $a_0 = 1$ . The constant first term on the right-hand side is determined by the scale factor and Hubble parameter at matter-radiation equality ( $a_{\text{eq}}, H_{\text{eq}}$ ) and the degrees of freedom in the thermal bath at  $a_{\text{eq}}$  and at reheating,  $g_*^{\text{eq}}$  and  $g_*^{\text{rh}}$ :

$$\ln \frac{a_{\text{eq}} H_{\text{eq}}}{a_0 H_0} - \frac{1}{4} \ln \frac{3H_{\text{eq}}^2}{M_{\text{P}}^2} - \frac{1}{12} \ln \frac{g_*^{\text{rh}}}{g_*^{\text{eq}}} = 66.64. \quad (32)$$

$H_{\text{eq}}$  and  $a_{\text{eq}}$  are determined by the matter density today,  $\Omega_m^0 = 0.3156$ , the red-shift of matter-radiation equality  $z_{\text{eq}} = 3395$  and the Hubble parameter today,  $H_0 = h 100 \text{ km s}^{-1} \text{ Mpc}^{-1}$ , with  $h = 0.6727$  [60]. As above  $g_*$  is set to the corresponding standard model values,  $g_*^{\text{rh}} = 427/4$  and  $g_*^{\text{eq}} = 43/11$ .

In the Monte Carlo scan we will impose the condition that  $N_*$  should lie within the interval

$$N_*^{\text{cond}} - 3 \leq N_* \leq N_*^{\text{cond}} + 3, \quad (33)$$

where we use  $\omega = 0$  as argued in Sec. 2.2. The reheating temperature is computed from Eq. (21) and the corresponding inflaton mass is obtained from  $V_{\text{end}}$  according to  $m_\phi^2 = \epsilon_{\text{end}} V_{\text{end}} / M_{\text{P}}^2$ . The latter corresponds to Eq. (14) if a single field  $\phi$  is responsible for driving inflation and reheating. If this is not the case, larger values of  $m_\phi$  and hence  $\rho_{\text{rh}}$  are possible. However  $N_*$  only depends very weakly on this quantity,  $\Delta N_* = (\ln \Delta \rho_{\text{rh}}) / 12$ . For simplicity we hence use the equality instead of the more general inequality in Eq. (14) for evaluating  $N_*$ , and take the uncertainty to be covered by allowing  $N_*$  to be in a finite range around  $N_*^{\text{cond}}$ , cf. Eq. (33). On the contrary, the lower bounds on  $V_{\text{end}}$  and  $T_{\text{rh}}$  (cf. Eq. (21)) are based on the more general inequality in Eq. (14), hence the results we present in Sec. 4 are

absolute lower bounds. If the operator of the inflaton decay is not specified we impose the conservative condition

$$N_*^{\text{cond}}(\text{dim } 6) - 3 \leq N_* \leq N_*^{\text{cond}}(\text{dim } 4) + 3, \quad (34)$$

with  $N_*^{\text{cond}}(\text{dim } 6)$  referring to Eq. (31) with  $\rho_{\text{rh}}$  expressed by means of the dimension six case in Eq. (21). Accordingly,  $N_*^{\text{cond}}(\text{dim } 4)$  corresponds to the dimension four (i.e. unsuppressed) case, i.e. removing  $m_\phi/M_{\text{P}}$  in Eq. (19). In both cases, we set the coupling constant  $\lambda$  to one.

### 3.4 Monte Carlo scan

In this subsection we briefly summarize the computational steps of the Monte Carlo scan over the parameter space spanned by the model (24), i.e., the parameters  $V_*, c_1, c_2, c_3, c_4$ . These parameters can be expressed as analytic functions of the CMB observables  $A_s, n_s, r, \alpha_s, \kappa_s$  to leading order in the slow-roll parameters (using (27)) in order to obtain an estimate of the parameter region of interest, which we use in the course of generating scan points as described below. However, after the generation of a parameter point we only keep the parameters  $V_*, c_1, c_2, c_3, c_4$  and recompute the CMB observables using the full expressions shown in the Appendix.

For each generated point of the Monte Carlo scan we perform the following steps. We first randomly choose  $A_s, n_s$  using a Gaussian probability distribution around their mean values (see Eq. (30)) with various widths up to 3 standard deviations as well as  $r$  with a logarithmically flat distribution between  $10^{-3}$  and 0.3. This determines  $V_*, c_1$  and  $c_2$  (at leading order in the slow-roll parameters). For variation of the coefficients  $c_3$  and  $c_4$ , determined by  $\alpha_s$  and  $\kappa_s$  at leading order in the slow-roll parameters, we follow three different approaches used for generating different sets of parameter points.

1. Randomly choosing  $\alpha_s$  and  $\kappa_s$  using a Gaussian probability distribution around their mean values (see Eq. (30)) with up to 2 standard deviations.
2. Randomly choosing  $c_3, c_4$  using a logarithmically flat probability distribution with different ranges between  $10^{-1}$  and  $10^{-15}$ .
3. Randomly choosing  $c_3, c_4$  close to values that lead to a vanishing discriminant (and discriminant of the discriminant) of the potential (see Sec. 3.5 for a detailed discussion).

The complete set of parameter points has been found to provide a sufficiently dense coverage of the region of large potential drops  $V_*/V_{\text{end}}$  and therefore ensures the formation of a sharp transition between forbidden and allowed points. Note that the absolute density of scan points does not claim any physical meaning.

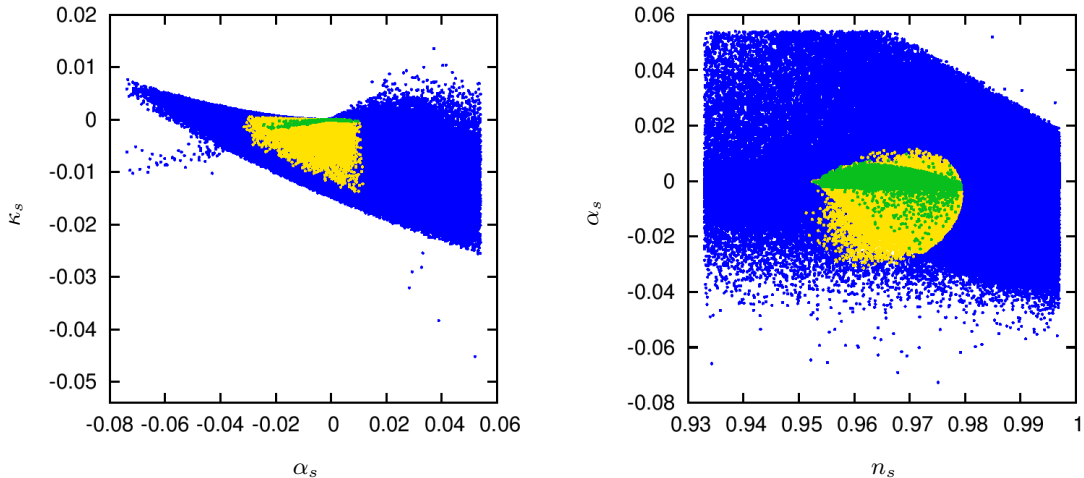


Figure 1: Scan points in terms of CMB observables. *Left panel:* Running ( $\alpha_s$ ) and running of the running ( $\kappa_s$ ) of the spectral index. *Right panel:* Spectral index  $n_s$  and its running  $\alpha_s$ . *Color-code:* Blue: Inflationary points. Yellow: Inflationary points within 2-sigma-contours regarding Planck data at  $\Delta\phi = 0$ . Green: Points additionally fulfilling the constraint on  $N_*$ .

For each point we then compute  $\Delta\phi_{\text{end}}$ , requiring

$$\epsilon(\Delta\phi_{\text{end}}) = \epsilon_{\text{end}}, \quad (35)$$

where we use  $\epsilon_{\text{end}} = 1$  (later we will also consider  $\epsilon_{\text{end}} = 3$  for an estimation of the systematic uncertainties due to the use of the slow-roll approximation, cf. also footnote 6). The solution of Eq. (35) only corresponds to a physical solution, if  $\Delta\phi_{\text{end}} < 0$ ,  $V'(\Delta\phi_{\text{end}}) > 0$  and if there is no zero of  $V'$  between 0 and  $\epsilon_{\text{end}}$ . Only points that fulfill these requirements are kept as potential inflationary points. For each potential inflationary point we compute  $N_*$  from

$$N_* = \int_{\Delta\phi_{\text{end}}}^0 \frac{V}{V'} \frac{d(\Delta\phi)}{M_{\text{P}}^2}. \quad (36)$$

Points with  $10 < N_* < 10^5$  are kept. Further we compute the  $\chi^2$  as described in Sec. 3.2 and impose the consistency condition for  $N_*$  arising from the comparison of the CMB pivot scale with the present Hubble horizon as detailed in Sec. 3.3. We generate a total of 15 million inflationary points.

Fig. 1 shows our scan points in the  $\alpha_s$ - $\kappa_s$  and  $n_s$ - $\alpha_s$  plane. Inflationary points (i.e. potentials which support slow-roll inflation for  $10 < N_* < 10^5$  e-folds) are marked in blue whilst points that additionally fulfill the Planck constraints on the scalar potential at  $\Delta\phi = 0$ , as described in Sec. 3.2, are marked in yellow. Note that these points do not represent potentials fully compatible with the Planck data, as the Planck data additionally contains the information that  $\Delta\phi = 0$  corresponds to a pivot scale of  $k_* = 0.002 \text{ Mpc}^{-1}$ . Rather these yellow



points (referred to as “locally Planck allowed” in the following) represent potentials which are locally consistent with the Planck data around  $\Delta\phi = 0$ , but in general will not give the observed amount of inflation between  $\Delta\phi = 0$  and  $\Delta\phi_{\text{end}}$ . This final condition is imposed by means of the consistency condition Eq. (34) and results in the points marked in green. As mentioned in Sec. 3.2 points that fulfill Eq. (34) only survive in a very small interval in  $\kappa_s$ . The stray blue points around  $\alpha_s \sim 0$ ,  $\kappa_s < -0.02$  in the left panel correspond to very small values of  $V_*/V_{\text{end}}$  and low values of  $N_*$ , close to the lower bound  $N_* > 10$ . Since this region of the parameter space is irrelevant for the lower bounds on  $V_{\text{end}}$  and  $T_{\text{rh}}$ , the density of scan points is very low here.

### 3.5 Properties of the inflaton potential

The parameter region of particular interest to this study is the regime which allows for the largest decrease of the potential energy during inflation. This implies a fairly steep potential allowing for a large energy drop during the final  $N_*$  e-folds while at the same time keeping the slow-roll parameters sufficiently small. In particular, not only must the derivatives of the potential be small compared to the inflationary scale  $V_*$ , but they must ‘track’ the rapidly falling energy density  $V(\Delta\phi)$  until after  $N_*$  e-folds the slow-roll parameter  $\epsilon$  reaches its critical value and inflation comes to an end. In Fig. 2 we schematically show the type of potentials which meet these requirements, as found in the Monte Carlo scan. Here, we have imposed the 95% confidence interval from the CMB data, cf. Sec. 3.2, and required values of  $N_*$  in accordance with Eq. (34). The color-coding refers to the tensor-to-scalar ratio  $r$ . We immediately notice that we can identify two different regimes, corresponding to potentials with minimum (blue) or saddle point (green) close to the end of inflation.

This can be understood as follows. As  $V(\Delta\phi)$  decreases towards the end of inflation, the slow-roll parameter  $\epsilon$  increases and inflation comes to an end – unless the numerator  $V'(\Delta\phi)$  of  $\epsilon$  vanishes simultaneously. The smallest values for  $V_{\text{end}}$  are hence achieved if  $V(\Delta\phi)$  and  $V'(\Delta\phi)$  have a common zero point at a suitable value of  $\Delta\phi$ . This implies an (at least) double zero point of  $V(\Delta\phi)$  and hence a necessary condition for the smallest  $V_{\text{end}}$  is a vanishing discriminant of  $V(\Delta\phi)$ . In practice, small values of  $V_{\text{end}}$  after a finite amount of e-folds are achieved if this condition is approximately satisfied, i.e. if the zero-points approximately coincide,

$$\text{Disc}[V(\Delta\phi)] \simeq 0. \quad (37)$$

Eq. (37) is an equation of degree three for the parameter  $c_4$  with generically one real and two complex solutions. We observe that potentials with particularly small  $V_{\text{end}}$  are achieved if (at

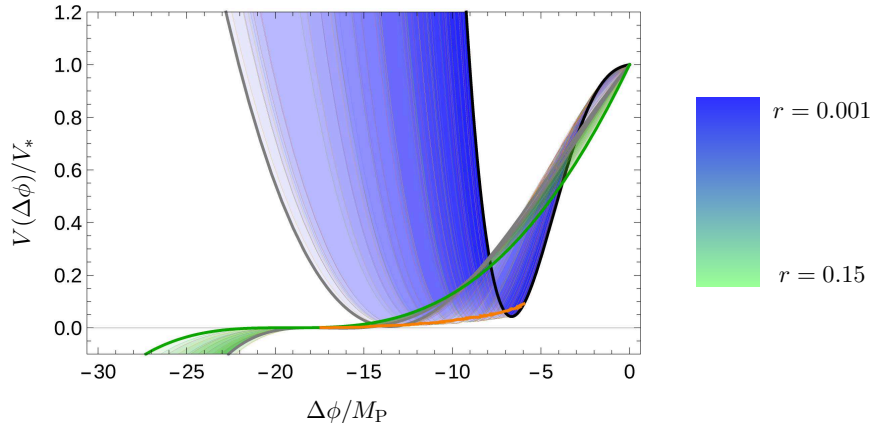


Figure 2: Scalar potentials which maximize the energy drop during the final  $N_*$  e-folds of inflation for different values of the tensor-to-scalar ratio  $r$  (color-coded on a logarithmic scale). The orange line marks the end of inflation at  $\epsilon = 1$ .

least) two of these solutions approximately coincide, i.e.

$$\text{Disc}[\text{Disc}[V(\Delta\phi)](c_4)] \simeq 0. \quad (38)$$

This condition implies that  $\text{Disc}[V(\Delta\phi)]$  has a double zero point at  $c_4^0 \in \mathbb{R}$ , ensuring that the smallness of  $\text{Disc}[V(\Delta\phi)]$  is stable against small variations of the parameter  $c_4$ , allowing us to find solutions for  $V(\Delta\phi)$  with (several) close, but not exactly coinciding zero-points – precisely what we are after. The two distinct situations observed in Fig. 2 correspond to potentials with two (blue) or three (green) almost coinciding zero-points. Four coinciding zero-points would simply correspond to a  $\phi^4$  potential, which is however clearly excluded by the Planck data. Eqs. (37) and (38) provide us with analytical solutions for two parameters ( $c_4$  and  $c_3$ ). Using values in the close vicinity of these solutions significantly increases the efficiency in exploring the large  $V_*/V_{\text{end}}$  region.

Moreover, we can exploit that certain ranges of the coefficients  $c_n$  lead to particularly large energy drops during inflation. For example, small values of the higher coefficients lead to well-behaved potentials, which are more likely to support inflation over a sufficient amount of e-folds. Also, we note that for small values of  $r$ , the  $\Delta\phi^3$ -coefficient is indirectly proportional to the square root of the tensor-to-scalar ratio,  $c_3 \propto -\alpha_s/\sqrt{r} \propto 1/c_1$ . This correlation is only strengthened by imposing the requirement on  $N_*$ . Implementing these observations allows us to efficiently investigate the region of large  $V_*/V_{\text{end}}$ .

## 4 Results and discussion

In this section, we present and discuss the results of the Monte Carlo scan. Following the strategy of the analytical discussion, cf. Sec. 2, we will first discuss the constraints on the scalar potential during the final  $N_*$  e-folds before drawing conclusions about the following reheating process.

### 4.1 The energy density at the end of inflation

The dynamics of inflation, described by Eq. (3), is independent of the overall scale  $V_*$  of the potential as defined in Eq. (24). As a first step, let us hence consider the relative drop of the scalar potential during inflation,  $V_*/V_{\text{end}}$ , as a function of  $N_*$  and  $r$ , respectively, cf. Fig. 3. Here we mark in blue all parameter points which sustain inflation for  $N_* = 10 - 10^5$  e-folds – implying that these potentials also contain a mechanism to end inflation by reaching  $\epsilon(\Delta\phi) = \epsilon_{\text{end}} = 1$ .<sup>11</sup> In yellow, we show the parameter points which additionally locally match the Planck data at 95% C.L., cf. Sec. 3.2. Finally in green, we impose the consistency condition on  $N_*$  given by Eq. (34). For comparison, the black dashed lines show the results obtained in Sec. 2 for the monomial potentials  $V \propto \phi^p$  and the exponential potential  $V \propto \exp(\sqrt{2\epsilon_{\text{end}}}\Delta\phi/M_{\text{P}})$ , cf. Eqs. (7) and (9). For monomials with  $p \leq 4$ , the red dashed lines indicate the range of  $N_*$ -values in accordance with Eq. (34).

Focusing on the locally Planck allowed points in the left panel, we first note that all points covered by our ansatz and locally allowed by the Planck data are far below the absolute upper bound for  $V_*/V_{\text{end}}$  given by the exponential potential. Moreover we can classify these points by the number of approximately coinciding zero-points at  $\Delta\phi \sim \Delta\phi_{\text{end}}$ , cf. Sec. 3.5. Points with one, two or three approximately coinciding zero-points are predominantly located in three horizontal bands yielding increasing values for  $V_*/V_{\text{end}}$ , roughly bounded from below by  $V_*/V_{\text{end}} = \{1, 25, 250\}$ , respectively, and broadening for increasing values of  $N_*$ . In the lowest band  $V(\Delta\phi)$  has a single (approximate) zero-point. As  $\Delta\phi$  approaches this value, the slow-roll parameter  $\epsilon$  blows up rapidly and inflation ends. The higher bands correspond to two and three (approximately) coinciding zero-points, i.e. common zero points in  $V(\Delta\phi)$  and  $V'(\Delta\phi)$ , allowing  $\epsilon$  to keep a finite value as  $V(\Delta\phi)$  approaches very small values. The monomial potentials with  $p = \{1, 2, 3\}$  can be seen as prototypical examples.

Also in the  $r$ - $V_*/V_{\text{end}}$  plane, the points locally allowed by the Planck constraint can be grouped according to number of coinciding zero-points, yielding three horizontal bands which turn upwards at  $r \sim 0.1 - 0.2$ . The structure of the resulting yellow region in the right panel

---

<sup>11</sup>In this sense, we restrict our analysis to single-field inflation models, excluding in particular models of hybrid inflation where the dynamics of a second scalar field is responsible for ending inflation.

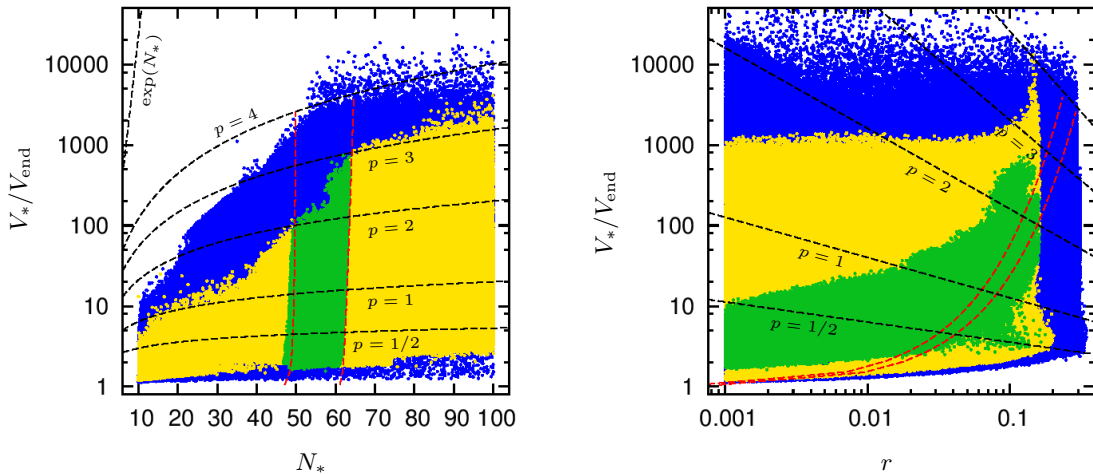


Figure 3: Scan points in the  $N_*$ - $(V_*/V_{\text{end}})$ -plane and  $r$ - $(V_*/V_{\text{end}})$ -plane. *Color-code*: Blue: Inflationary points. Yellow: Inflationary points within 2-sigma-contours regarding Planck data at  $\Delta\phi = 0$ . Green: Points additionally fulfilling the constraint on  $N_*$ . Dashed black curves: Prediction for monomial potentials  $\phi^p$  with the constraint on  $N_*$  fulfilled within the region marked dashed red (for  $p \leq 4$ ). In the left panel, we additionally show the most conservative analytical bound, the exponential potential.

of Fig. 3 can be understood based on Eq. (37). Taking  $\alpha_s$  and  $\kappa_s$  to be close to zero as indicated by the Planck data and  $n_s$  within the  $2\sigma$  region,  $\text{Disc}[V(\Delta\phi), \Delta\phi]$  is approximately constant for small  $r$  until reaching a zero-point around  $r \sim 0.11$ - $0.23$ . In this region of large  $r$ , very small values of  $\text{Disc}[V(\Delta\phi), \Delta\phi]$  are reached, corresponding to (several) nearly coinciding zero-points allowing for large  $V_*/V_{\text{end}}$ . In this sense, the recent Planck results have now reached a crucial sensitivity, excluding the part of the parameter space where  $V_*/V_{\text{end}}$  begins to shoot up. Correspondingly, if future measurements are able to constrain the tensor-to-scalar ratio to be below about  $r \sim 0.05$ , the upper bound on  $V_*/V_{\text{end}}$  will become about an order of magnitude stricter. The overall shape of the green region can be understood by employing monomial potentials as prototypical examples. High values of  $V_*/V_{\text{end}}$  are reached if  $V(\Delta\phi)$  has a multiple zero-point ( $p \geq 2$ , corresponding to a sizable value of  $r$ ) whereas at small values of  $r$ , for  $p \ll 1$ , the potential becomes very flat and  $V_*/V_{\text{end}} \rightarrow 1$ .

From the discussion above we can anticipate that the parameter points with high  $V_*/V_{\text{end}}$  come with finely tuned parameters. To quantify this, we determine the fine-tuning measure [61]

$$\xi \equiv \text{Max} \left[ \frac{\delta(V_*/V_{\text{end}})}{\delta c_n} \frac{c_n}{(V_*/V_{\text{end}})}, n = 1, \dots, 4 \right], \quad (39)$$

with  $\delta c_n$  denoting a small variation of the respective parameter of the scalar potential (24),  $|\delta c_n/c_n| \sim 10^{-6}$ . Large values of  $\xi$  indicate a high degree of fine-tuning, implying that the value of  $V_*/V_{\text{end}}$  is extremely sensitive to at least one of the parameters. On the other hand,

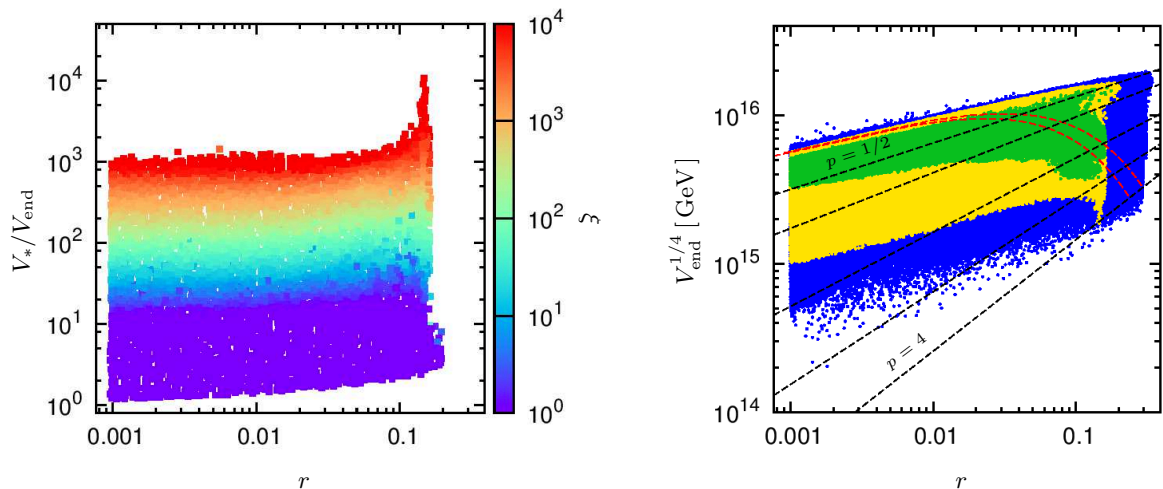


Figure 4: Fine-tuning  $\xi$  among the locally Planck allowed points in the  $r$ - $(V_*/V_{\text{end}})$ -plane (left) and lower bound on the energy density at the end of inflation in the  $r$ - $V_{\text{end}}$ -plane (right). The color-code in the right panel is as in Fig. 3.

points with  $\xi = \mathcal{O}(1-10)$  correspond to potentials which do not require any particular tuning. In the left panel of Fig. 4 we show the fine-tuning measure  $\xi$  where we performed a binning among the locally Planck allowed points in the  $r$ - $(V_*/V_{\text{end}})$  plane and displayed the point with the smallest value of  $\xi$  in each bin. As expected, high values of  $V_*/V_{\text{end}}$  always come with a high degree of tuning. This is rather independent of the value of  $r$ . In particular, the three horizontal ‘bands’ mentioned above, corresponding to an increasing number of coinciding zero-points, are also clearly distinguished by increasingly higher fine-tuning. Dropping the requirement of lying within the 2-sigma-region of the Planck data and considering the full data set, we observe that the fine-tuning is relaxed for small  $r$  by up to a factor of 10 but remains basically unchanged for  $r \sim 0.1$ . The high tuning is hence mainly a result of the careful balance of  $V$  and  $V'$  in the slow-roll parameter  $\epsilon$ , and is not a feature of the specific values of the CMB observables, in particular for large values of  $r$ . Comparing the left panel of Fig. 4 with the points passing all constraints in the right panel of Fig. 3, we note that in particular the large values of  $V_*/V_{\text{end}}$  around  $r \sim 0.1$  feature a maybe uncomfortably high degree of tuning. A restriction to less severely tuned potential would correspondingly yield a tighter upper bound on  $V_*/V_{\text{end}}$ , translating to a tighter lower bound on the reheating temperature. Since choosing the acceptable degree of tuning is however a very subjective question, we continue in the following with the full data set.

Finally, in the right panel of Fig. 4, we include the information on  $V_*$  which comes with an additional  $r$ -dependence. This leads to the final constraints on the energy density at the end of inflation, one of the main results of this paper. Independent of any assumptions about

the reheating process which we will make in the following section, we find that the CMB observations constrain this energy scale to  $3 \times 10^{15} \text{ GeV} < (V_{\text{end}})^{1/4} < 2 \times 10^{16} \text{ GeV}$  for  $r > 10^{-3}$  for the scalar potential of any single-field inflation model described by operators up to dimension four. This remarkable narrow range close the GUT scale might be taken as an indication to explore connections between inflation and the breaking of a unified gauge group. While this has been recently much discussed in the context of a large tensor-to-scalar ratio, we stress that indeed this conclusion holds over the entire range of the tensor-to-scalar ratios investigated,  $0.001 < r < 0.15$ , since the overall scaling of the potential,  $V_* \propto r$ , is to some extent compensated by the large decrease in energy allowed by large  $r$ . This is illustrated by the example of the monomial potentials, cf. dashed red lines in Fig. 4. For small values of  $r$ , the drop in energy during inflation becomes negligible and the energy at the end of inflation is mainly determined by the  $r$ -dependence of  $V_*$ . As an aside, we point out that this provides a good indication on how to extend our bounds to smaller values of  $r < 10^{-3}$ . The results depicted in the right panel of Fig. 4 stress the importance of upcoming CMB experiments. The detection of a tensor-to-scalar ratio in the percent regime,  $0.01 \leq r \leq 0.06$ , would tighten the bound on the energy density at the end of inflation to  $(V_{\text{end}})^{1/4} > 5 \times 10^{15} \text{ GeV}$ .

Bounds on the scalar potential of inflation have been derived in other contexts. Using the same ansatz as Eq. (24), the Planck collaboration recently performed a local reconstruction of the scalar potential around  $\phi_*$ , restricting themselves to the observable part of the potential [1]. We find that our ranges for the parameters  $c_n$  lie well within the ranges found in this local reconstruction. This is an important cross-check, implying that also a few e-folds before the pivot-scale our potentials are sufficiently well behaved to not generate any anomalies at low multipoles in the CMB. Compared to Ref. [1], our parameter ranges are of course much more constrained since we additionally impose the requirement that extending Eq. (24) to large values of  $\Delta\phi$ , the scalar potential supports slow-roll inflation for a suitable amount of e-folds. Moreover, recently in Ref. [58] a lower bound on  $V_*/V_{\text{end}}$  was derived,  $V_*/V_{\text{end}} > 1.01$  for  $r < 0.15$ , in this sense focussing on the opposite limit as the bound presented here.

## 4.2 A lower bound on the reheating temperature

Equipped with a lower bound on the energy scale at the end of inflation,  $V_{\text{end}}$ , we can proceed to constrain the reheating temperature based on Eqs. (14) and (21). In Fig. 5 we show the resulting lower bound on  $T_{\text{rh}}$  based on a dimension five and dimension six operator for the inflaton decay, respectively. Based on the monomials as prototypical examples the overall scale and shape of this constraint is well understood by applying Eq. (23). In both cases, we

obtain values significantly above the BBN constraint of about 10 MeV,

$$\begin{aligned} T_{\text{rh}}^{\text{dim } 5} &> 3 \times 10^8 \text{ GeV}, \\ T_{\text{rh}}^{\text{dim } 6} &> 7 \times 10^2 \text{ GeV}. \end{aligned} \tag{40}$$

for  $r > 0.001$ . Here, as in Fig. 5, we have set the coupling constant in Eq. (21) to  $\lambda = 1$ . Note that  $T_{\text{rh}}$  depends linearly on  $\lambda$ , hence a suppression of this coupling constant can weaken the bound accordingly.

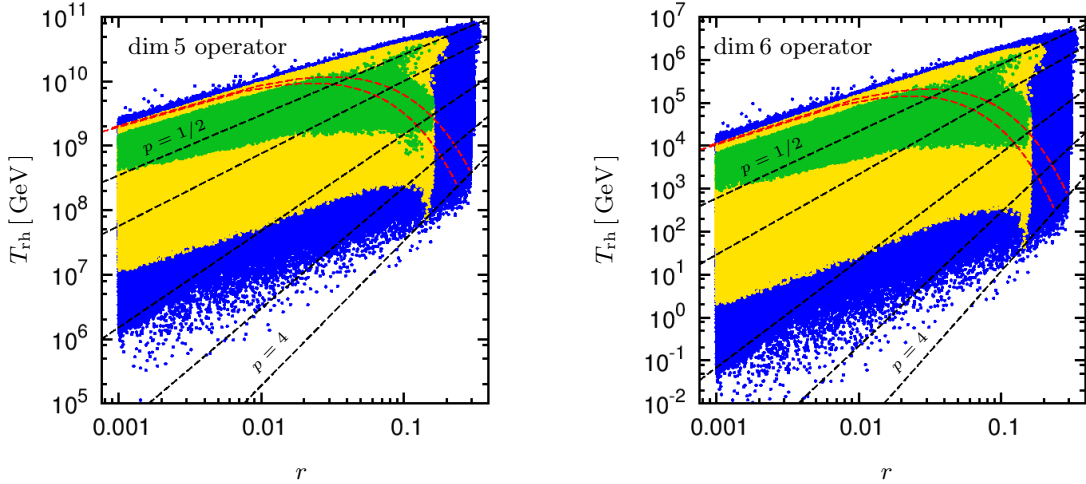


Figure 5: Scan points in the  $r$ - $T_{\text{rh}}$ -plane showing the lower bound on the reheating temperature for a decay via dimension five operators (left) and dimension six operator (right) with  $\lambda = 1$ . The color-code is as in Fig. 3.

The left panel of Fig. 5 displays a remarkably strong bound for the dimension five case, implying that temperatures at least very close to the temperatures relevant for the gravitino problem and thermal leptogenesis were indeed reached in the early universe ( $T \sim 10^9$  GeV). This bound might be further tightened if upcoming B-mode searches succeed in detecting a tensor-to-scalar ratio of a few percent,  $0.01 < r < 0.07$ . In this region, the lower bound on the reheating temperature for  $\lambda = 1$  reaches as high as  $T_{\text{rh}} > (1-2) \times 10^9$  GeV. This bound is however significantly weakened if the coupling  $\lambda$  is suppressed, either by a symmetry or by an accidentally small value. To demonstrate this effect, we consider the situation where the dimension five operator is negligibly small and the time-scale of reheating is instead governed by a dimension six operator in the right panel of Fig. 5. In this case the constraint on the reheating temperature is significantly weaker, owing to the additional factor of  $m_\phi/M_{\text{P}} \sim \sqrt{V_{\text{end}}}/M_{\text{P}}^2$ , but is still well above the BBN bound of 10 MeV.

Throughout this study we have employed  $\epsilon = 1$  as the condition for the end of inflation. Since slow-roll is violated at the end of inflation, this is however only approximately correct, more precisely inflation ends at  $\epsilon_H = \dot{\phi}^2/(2H^2) = 1$  [38]. The effect of this on the bounds

derived on the quantities of the reheating process is discussed in footnote 6, here we comment on the resulting uncertainty of the quantities  $V_*/V_{\text{end}}$  and  $T_{\text{rh}}$  due to a misestimation of  $\Delta\phi_{\text{end}}$ . To this end we have solved the full second order differential equation (10) for a representative subset of 20000 parameter points.<sup>12</sup> (Unfortunately, applying this procedure in the full parameter scan is computationally too demanding.) As expected, we find  $\epsilon(\epsilon_H = 1) \gtrsim 1$ , hence the slow-roll approximation underestimates  $\Delta\phi_{\text{end}}$  and thus  $V_*/V_{\text{end}}$ . We find that without the slow-roll approximation,  $N_*$  increases by  $\Delta N_* = 1.1 - 2.2$  and  $V_*/V_{\text{end}}$  increases by an  $\mathcal{O}(1)$  factor, which in the most interesting range  $45 < N_* < 65$  is found to be  $(V_*/V_{\text{end}})_{\text{full}}/(V_*/V_{\text{end}})_{\text{sr}} \simeq 1.8 - 2.1$ . We observe that since  $\epsilon$  grows very rapidly at the end of inflation in the models of interest here, the errors in  $\Delta\phi_{\text{end}}$  and the derived quantities are small. The bound (14) on  $m_\phi$ , entering the bounds on the reheating temperature via Eq. (21), changes by a factor of 0.7 - 1.8. This moderate change is due to compensating effects of  $\epsilon_{\text{end}}$ , which increases, and  $V_{\text{end}}$ , which decreases with respect to the slow-roll approximation. In summary the uncertainty arising from the use of the slow-roll approximation is very moderate.

In the analysis presented here, we have restricted ourselves to a matter-dominated reheating phase,  $\omega = 0$ , while allowing for a wide range of inflationary potentials.<sup>13</sup> An alternative approach to constrain the reheating temperature is to fix the inflation model and then use Eq. (31) to constrain the reheating temperature. This allows one to probe all reheating scenarios with a constant  $\omega$ . A recent analysis along these lines can be found in Ref. [27]. For simple inflationary models, such as the monomial potentials which have served as prototypical examples throughout this paper, the resulting bounds on the reheating temperature can be determined analytically. For a  $\phi^2$  monomial potential and  $\omega = 0$ , the reheating temperature is found to be larger than about  $10^9$  GeV from the  $1\sigma$  constraints on the spectral index  $n_s$ , consistent with our results. However, lowering the power of the monomial to  $p = 1$ , the bound completely disappears, allowing for reheating temperatures in the full range of  $10 \text{ MeV} < T_{\text{rh}} < 2 \times 10^{16} \text{ GeV}$ . The result is also very sensitive to the choice of  $\omega$ , increasing its value to  $\omega = 2/3$  implies for the  $p = 2$  case that no significant bounds can be placed on the reheating temperature, whereas for  $\omega = -1/3$  the lower bound is raised to about  $10^{14}$  GeV. While it is remarkable that the CMB data alone can yield strong constraints on the reheating temperature for certain inflation models, these results also stress the need for a more model independent approach, as we have pursued in this paper.

Further approaches to constrain the reheating temperature include constraints from the

---

<sup>12</sup>To obtain robust statements, we consider three different parameter sets: After binning our points in the  $r$ - $(V_*/V_{\text{end}})$  plane, we consider first a randomly chosen point within each bin and, second, the point with the highest and lowest fine-tuning, respectively. Third, we re-compute our results for  $\epsilon_{\text{end}} = 3$  (which is found to be a typical value for  $\epsilon(\epsilon_H = 1)$ ), and select the allowed points with highest  $V_*/V_{\text{end}}$ .

<sup>13</sup>Note that as argued around Eq. (16), we expect the dependence of our analysis on the value  $\omega$  to be small.



thermalization of neutrinos, measured by the effective number neutrinos  $N_{\text{eff}}$  required to reproduce the CMB spectrum [62, 63], implying however only a rather weak bound of  $T_{\text{rh}} > 3.2$  MeV. Moreover, a detection of gravitational waves by future space-based experiments such as BBO [64] and DECIGO [65] would open a completely new window to the energy scales of the early universe. Given a sufficiently large tensor-to-scalar ratio, this would allow to probe the reheating in a range of  $10^6 - 10^9$  GeV [66]. Finally, from a theoretical point of view it has been argued that there is an upper bound on the reheating temperature,  $T < 10^9$  GeV, since large couplings of the inflaton field to any other particles would destroy the flatness of the inflaton potential via radiative corrections [32]. This bound can however easily be avoided if the time-scale of reheating is set by the decay of a particle different than the inflaton, as can occur e.g. in hybrid inflation or in some preheating scenarios.

## 5 Conclusion

In this paper we derived constraints on the relevant energy scales of the very early universe, namely the energy scale at the end of inflation,  $V_{\text{end}}$ , the mass of the inflaton,  $m_\phi$ , and the reheating temperature,  $T_{\text{rh}}$ . The most dramatic potential drop  $V_*/V_{\text{end}}$  is realized in an exponential potential yielding the most conservative bound  $V_*/V_{\text{end}} < e^{N_*}$ . However, for a realistic single-field inflation scenario – providing a mechanism to end inflation as well as being consistent with observations of the CMB around the pivot scale – a much stronger bound can be achieved. In order to cover a large class of relevant inflation models we examined a general fourth order polynomial potential. We constrained this potential by requiring consistency with recent data from the Planck collaboration and by demanding that inflation ends after the number of e-folds which provides a matching between the CMB pivot scale and today’s Hubble horizon. We found that this restricts the potential drop to stay below  $V_*/V_{\text{end}} \simeq 1000$ , yielding the highest values for large tensor-to-scalar-ratios close to being excluded by Planck,  $r \simeq 0.1$ . For smaller  $r$  the potential drop becomes significantly smaller. This results in the bound  $V_{\text{end}}^{1/4} > 3 \times 10^{15}$  GeV for  $r > 0.001$  – remarkably close to the GUT scale.

Matching the inflaton potential at the end of inflation to the subsequent oscillation phase allowed us to connect  $V_{\text{end}}$  and  $m_\phi$  which provides a lower bound on the inflaton mass. This allows us in turn to estimate the decay width of the inflaton governing the time scale of the energy transition to the thermal bath and hence the energy density at the beginning of the radiation dominated phase. Without taking into account the decay width of the inflaton, the reheating temperature can only be constrained by solving Eq. (31) for  $\rho_{\text{rh}}$ . However, due to the logarithmic dependence this procedure is subject to huge uncertainties, in particular it does not provide an interesting bound in the general class of models considered in this

paper. Instead we specified the decay mode of the inflaton by exemplarily considering generic Planck-suppressed dimension five and six operators. This allowed us to place bounds on the reheating temperature,  $T_{\text{rh}}^{\text{dim}5} > 3 \times 10^8$  GeV and  $T_{\text{rh}}^{\text{dim}6} > 7 \times 10^2$  GeV, significantly above the requirement that thermalization of the universe has to take place well before BBN,  $T_{\text{rh}} > 10$  MeV. If moreover upcoming B-mode searches succeed in detecting a tensor-to-scalar ratio of a few percent,  $0.01 < r < 0.07$ , our results imply a particularly interesting bound in the dimension five case,  $T_{\text{rh}} > 10^9$  GeV. For a reheating temperature in this range, the gravitino problem provides very challenging limitation on the supersymmetric parameter space.

We emphasize that our results are robust in various concerns. The derived bounds do not depend strongly on the choice of  $\epsilon_{\text{end}}$ . Although our results are achieved for single-field inflation models we expect the bounds to conservatively hold for the situation in which inflation is ended by a second field and hence  $\epsilon_{\text{end}}$  is not required to become large towards the end of inflation. In order to match the inflaton potential at the end of inflation to the subsequent oscillation phase we assumed a (predominantly) quadratic potential in the latter phase, i.e. an equation of state  $\omega = 0$ . We argued that even for a different choice of  $\omega$  our results are not changed significantly. Throughout this study we worked in the slow-roll approximation. Nevertheless we have discussed that our bounds are expected to hold up to an  $\mathcal{O}(1)$  factor even if the slow-roll conditions are slightly violated. In contrast to the robustness of the bound on  $V_{\text{end}}$  there, however, remains a huge dependence of the bound on  $T_{\text{rh}}$  to an unknown quantity, namely the type and coefficient of the operator governing the inflaton decay. This amounts in a difference of almost six orders of magnitude between the case of a dimension five and six operator.

## Acknowledgements

We thank Stefan Antusch, Marco Drewes, Julien Lesgourgues, David Nolde, Martin Schmaltz and Alexander Westphal for very helpful discussions. This work was supported by the European Union Program FP7 ITN INVISIBLES (Marie Curie Actions, PITN-GA-2011-289442).

## Appendix

### A CMB observables beyond leading order

In this Appendix we present the full expressions for the CMB observables in terms of the potential slow-roll parameters used for the computation of  $\chi^2$  as described in Sec. 3.2. In all expressions the slow-roll parameters are evaluate at  $\phi = \phi_*$ . Note that there does not exist a slow-roll parameter beyond  $\sigma^3$  for the considered class of potentials (24) as the fifth derivative of the potential vanishes. To second order in the slow-roll parameters the scalar amplitude reads [67]

$$A_s = \frac{V}{24\pi^2\epsilon M_{\text{P}}^4} \left[ 1 + \left( -\frac{1}{3} - 6C \right) \epsilon + \left( -\frac{2}{3} + 2C \right) \eta + \left( -\frac{154}{3} + \frac{11\pi^2}{2} - \frac{4C}{3} + 6C^2 \right) \epsilon^2 + \left( \frac{284}{9} - \frac{11\pi^2}{3} + \frac{4C}{3} - 4C^2 \right) \epsilon\eta + \left( -\frac{37}{9} + \frac{\pi^2}{2} - \frac{2C}{3} + 2C^2 \right) \eta^2 + \left( -\frac{2}{9} + \frac{\pi^2}{12} + \frac{2C}{3} - C^2 \right) \xi^2 \right]. \quad (41)$$

In the above expressions we introduced

$$C = -2 + \ln 2 + \gamma_{\text{E}} \simeq -0.729637, \quad (42)$$

where  $\gamma_{\text{E}}$  is the Euler-Mascheroni constant,  $\gamma_{\text{E}} \simeq 0.577216$ . From  $A_s$  we can compute

$$n_s - 1 = \frac{d \ln A_s}{d \ln k}, \quad (43)$$

$$\alpha_s = \frac{dn_s}{d \ln k}, \quad (44)$$

$$\kappa_s = \frac{d\alpha_s}{d \ln k}, \quad (45)$$

using the general relation [67]

$$\frac{dX|_{aH=k}}{d \ln k} = - \left( 1 + \frac{1}{3}\epsilon + \frac{1}{3}\eta + \frac{5}{9}\epsilon^2 - \frac{4}{9}\epsilon\eta + \frac{2}{9}\eta^2 + \frac{1}{9}\xi^2 + \mathcal{O}(\epsilon^3) \right) \frac{V'}{V} \frac{dX}{d\phi} \Big|_{aH=k}. \quad (46)$$

We obtain

$$n_s = 1 - 6\epsilon + 2\eta + \left( -\frac{10}{3} - 24C \right) \epsilon^2 - (2 - 16C)\epsilon\eta + \frac{2}{3}\eta^2 + \left( \frac{2}{3} - 2C \right) \xi^2 + \left( -\frac{3734}{9} - \frac{104C}{3} - 96C^2 + 44\pi^2 \right) \epsilon^3 + \left( \frac{1190}{3} - \frac{4C}{3} + 96C^2 - 44\pi^2 \right) \epsilon^2\eta + \left( -\frac{742}{9} + 12C - 16C^2 + \frac{28\pi^2}{3} \right) \epsilon\eta^2 + \frac{4}{9}\eta^3 + \left( -\frac{98}{3} + 4C - 12C^2 + 4\pi^2 \right) \epsilon\xi^2 + \left( \frac{28}{3} - \frac{8C}{3} + C^2 - \frac{13\pi^2}{12} \right) \eta\xi^2 + \left( \frac{2}{9} - \frac{2C}{3} + C^2 - \frac{\pi^2}{12} \right) \sigma^3, \quad (47)$$

$$\begin{aligned}
\alpha_s = & -24\epsilon^2 + 16\epsilon\eta - 2\xi^2 - \\
& \left(\frac{104}{3} + 192C\right)\epsilon^3 - \left(\frac{4}{3} - 192C\right)\epsilon^2\eta + 4(3 - 8C)\epsilon\eta^2 + (4 - 24C)\epsilon\xi^2 - \\
& \left(\frac{8}{3} - 2C\right)\eta\xi^2 - \left(\frac{2}{3} - 2C\right)\sigma^3 - \\
& \left(+\frac{45008}{9} + 480C + 1152C^2 - 528\pi^2\right)\epsilon^4 + \left(\frac{58204}{9} + \frac{584C}{3} + 1536C^2 - 704\pi^2\right)\epsilon^3\eta - \\
& \left(2256 - \frac{464C}{3} + 512C^2 - \frac{752\pi^2}{3}\right)\epsilon^2\eta^2 + \left(\frac{520}{3} - \frac{104C}{3} + 32C^2 - \frac{56\pi^2}{3}\right)\epsilon\eta^3 - \\
& \left(\frac{5942}{9} - \frac{76C}{3} + 192C^2 - 76\pi^2\right)\epsilon^2\xi^2 + \left(\frac{2902}{9} - \frac{178C}{3} + 74C^2 - \frac{223\pi^2}{6}\right)\epsilon\eta\xi^2 + \\
& \left(-\frac{106}{9} + \frac{10C}{3} - C^2 + \frac{13\pi^2}{12}\right)\eta^2\xi^2 - \left(\frac{86}{9} - \frac{8C}{3} + C^2 - \frac{13\pi^2}{12}\right)\xi^4 - \\
& \left(\frac{304}{9} - \frac{22C}{3} + 18C^2 - \frac{9\pi^2}{2}\right)\epsilon\sigma^3 + \left(-10 + \frac{14C}{3} - 3C^2 + \frac{5\pi^2}{4}\right)\eta\sigma^3,
\end{aligned} \tag{48}$$

$$\begin{aligned}
\kappa_s = & -192\epsilon^3 + 192\epsilon^2\eta - 32\epsilon\eta^2 - 24\epsilon\xi^2 + 2\eta\xi^2 + 2\sigma^3 - \\
& (480 + 2304C)\epsilon^4 + \left(\frac{584}{3} + 3072C\right)\epsilon^3\eta + \left(\frac{464}{3} - 1024C\right)\epsilon^2\eta^2 - \\
& \left(\frac{104}{3} - 64C\right)\epsilon\eta^3 + \left(\frac{76}{3} - 384C\right)\epsilon^2\xi^2 - \left(\frac{178}{3} - 148C\right)\epsilon\eta\xi^2 + \\
& \left(\frac{10}{3} - 2C\right)\eta^2\xi^2 + \left(\frac{8}{3} - 2C\right)\xi^4 - \left(\frac{22}{3} - 36C\right)\epsilon\sigma^3 + \left(\frac{14}{3} - 6C\right)\eta\sigma^3 - \\
& \left(\frac{722336}{9} + 8448C + 18432C^2 - 8448\pi^2\right)\epsilon^5 + \\
& \left(\frac{1175984}{9} + \frac{20464C}{3} + 30720C^2 - 14080\pi^2\right)\epsilon^4\eta - \\
& \left(\frac{593296}{9} - \frac{4112C}{3} + 15360C^2 - 7232\pi^2\right)\epsilon^3\eta^2 + \\
& \left(10840 - \frac{3856C}{3} + 2368C^2 - \frac{3568\pi^2}{3}\right)\epsilon^2\eta^3 - \\
& \left(\frac{3256}{9} - \frac{272C}{3} + 64C^2 - \frac{112\pi^2}{3}\right)\epsilon\eta^4 - \\
& \left(\frac{43240}{3} + \frac{56C}{3} + 3840C^2 - 1616\pi^2\right)\epsilon^3\xi^2 + \\
& \left(\frac{99580}{9} - 1108C + 2724C^2 - 1253\pi^2\right)\epsilon^2\eta\xi^2 - \\
& \left(\frac{14470}{9} - \frac{1072C}{3} + 326C^2 - \frac{1057\pi^2}{6}\right)\epsilon\eta^2\xi^2 + \\
& \left(\frac{118}{9} - 4C + C^2 - \frac{13\pi^2}{12}\right)\eta^3\xi^2 - \left(\frac{1202}{3} - 80C + 82C^2 - \frac{275\pi^2}{6}\right)\epsilon\xi^4 + \\
& \left(\frac{394}{9} - \frac{38C}{3} + 4C^2 - \frac{13\pi^2}{3}\right)\eta\xi^4 + \left(\frac{8968}{9} - \frac{260C}{3} + 372C^2 - 121\pi^2\right)\epsilon^2\sigma^3 - \\
& \left(\frac{4858}{9} - 136C + 170C^2 - \frac{391\pi^2}{6}\right)\epsilon\eta\sigma^3 + \\
& \left(\frac{302}{9} - \frac{44C}{3} + 7C^2 - \frac{43\pi^2}{12}\right)\eta^2\sigma^3 + \left(\frac{88}{3} - 10C + 5C^2 - \frac{41\pi^2}{12}\right)\xi^2\sigma^3.
\end{aligned} \tag{49}$$

Using the results from [68] and [67] we can obtain a second order expression for the tensor-to-scalar ratio:

$$r = 16\epsilon - \left(\frac{64}{3} - 64C\right)\epsilon^2 + \left(\frac{32}{3} - 32C\right)\epsilon\eta. \tag{50}$$

## References

- [1] Planck Collaboration, P. Ade *et al.*, “Planck 2015. XX. Constraints on inflation”, [arXiv:1502.02114](#) [astro-ph.CO].
- [2] J. Martin, C. Ringeval, and V. Vennin, “Encyclopædia Inflationaris”, *Phys. Dark Univ.* **5-6** (2014) 75–235, [arXiv:1303.3787](#) [astro-ph.CO].
- [3] N. Okada, V. N. enouz, and Q. Shafi, “Simple Inflationary Models in Light of BICEP2: an Update”, [arXiv:1403.6403](#) [hep-ph].
- [4] BICEP2, Planck, P. Ade *et al.*, “Joint Analysis of BICEP2/Keck Array and Planck Data”, *Phys. Rev. Lett.* **114** (2015) 101301, [arXiv:1502.00612](#) [astro-ph.CO].
- [5] T. Essinger-Hileman, J. Appel, J. Beall, H. Cho, J. Fowler, *et al.*, “The Atacama B-Mode Search: CMB Polarimetry with Transition-Edge-Sensor Bolometers”, [arXiv:1008.3915](#) [astro-ph.IM].
- [6] J. Errard, “The new generation CMB B-mode polarization experiment: POLARBEAR”, in *2010 Rencontres de Moriond proceedings*. 2010. [arXiv:1011.0763](#) [astro-ph.IM].
- [7] C. Sheehy, P. Ade, R. Aikin, M. Amiri, S. Benton, *et al.*, “The Keck Array: a pulse tube cooled CMB polarimeter”, [arXiv:1104.5516](#) [astro-ph.IM].
- [8] M. Fukugita and T. Yanagida, “Baryogenesis Without Grand Unification”, *Phys.Lett.* **B174** (1986) 45.
- [9] W. Buchmuller, P. Di Bari, and M. Plumacher, “Leptogenesis for pedestrians”, *Annals Phys.* **315** (2005) 305–351, [arXiv:hep-ph/0401240](#) [hep-ph].
- [10] P. Fayet, “Experimental consequences of supersymmetry”, in *Proceedings of the XVIth Rencontre de Moriond*, J. Tran Thanh Van, ed., vol. 1, pp. 347–367. Editions Frontieres, 1981.
- [11] H. Pagels and J. R. Primack, “Supersymmetry, Cosmology and New TeV Physics”, *Phys.Rev.Lett.* **48** (1982) 223.
- [12] S. Weinberg, “Cosmological Constraints on the Scale of Supersymmetry Breaking”, *Phys.Rev.Lett.* **48** (1982) 1303.
- [13] J. R. Ellis, D. V. Nanopoulos, and S. Sarkar, “The Cosmology of Decaying Gravitinos”, *Nucl.Phys.* **B259** (1985) 175.

- [14] M. Kawasaki, K. Kohri, and T. Moroi, “Hadronic decay of late - decaying particles and Big-Bang Nucleosynthesis”, *Phys.Lett.* **B625** (2005) 7–12, [arXiv:astro-ph/0402490](#) [astro-ph].
- [15] M. Kawasaki, K. Kohri, and T. Moroi, “Big-Bang nucleosynthesis and hadronic decay of long-lived massive particles”, *Phys.Rev.* **D71** (2005) 083502, [arXiv:astro-ph/0408426](#) [astro-ph].
- [16] K. Jedamzik, “Big bang nucleosynthesis constraints on hadronically and electromagnetically decaying relic neutral particles”, *Phys.Rev.* **D74** (2006) 103509, [arXiv:hep-ph/0604251](#) [hep-ph].
- [17] T. Moroi, H. Murayama, and M. Yamaguchi, “Cosmological constraints on the light stable gravitino”, *Phys.Lett.* **B303** (1993) 289–294.
- [18] J. Pradler and F. D. Steffen, “Constraints on the Reheating Temperature in Gravitino Dark Matter Scenarios”, *Phys. Lett.* **B648** (2007) 224–235, [arXiv:hep-ph/0612291](#).
- [19] T. Asaka, K. Hamaguchi, and K. Suzuki, “Cosmological gravitino problem in gauge mediated supersymmetry breaking models”, *Phys. Lett.* **B490** (2000) 136–146, [arXiv:hep-ph/0005136](#).
- [20] F. D. Steffen, “Probing the Reheating Temperature at Colliders and with Primordial Nucleosynthesis”, *Phys. Lett.* **B669** (2008) 74–80, [arXiv:0806.3266](#) [hep-ph].
- [21] L. Covi, M. Olechowski, S. Pokorski, K. Turzyski, and J. D. Wells, “Supersymmetric mass spectra for gravitino dark matter with a high reheating temperature”, *JHEP* **1101** (2011) 033, [arXiv:1009.3801](#) [hep-ph].
- [22] L. Roszkowski, S. Trojanowski, K. Turzyski, and K. Jedamzik, “Gravitino dark matter with constraints from Higgs boson mass and sneutrino decays”, *JHEP* **1303** (2013) 013, [arXiv:1212.5587](#).
- [23] J. Heisig, “Gravitino LSP and leptogenesis after the first LHC results”, *JCAP* **1404** (2014) 023, [arXiv:1310.6352](#) [hep-ph].
- [24] J. Lesgourgues and W. Valkenburg, “New constraints on the observable inflaton potential from WMAP and SDSS”, *Phys.Rev.* **D75** (2007) 123519, [arXiv:astro-ph/0703625](#) [ASTRO-PH].
- [25] W. H. Kinney, “Inflation: Flow, fixed points and observables to arbitrary order in slow roll”, *Phys.Rev.* **D66** (2002) 083508, [arXiv:astro-ph/0206032](#) [astro-ph].

- [26] J. Martin and C. Ringeval, “First CMB Constraints on the Inflationary Reheating Temperature”, *Phys.Rev.* **D82** (2010) 023511, [arXiv:1004.5525 \[astro-ph.CO\]](#).
- [27] J. L. Cook, E. Dimastrogiovanni, D. A. Easson, and L. M. Krauss, “Reheating predictions in single field inflation”, *JCAP* **1504** (2015) 047, [arXiv:1502.04673 \[astro-ph.CO\]](#).
- [28] J. Martin, C. Ringeval, and V. Vennin, “Observing Inflationary Reheating”, *Phys.Rev.Lett.* **114** (2015) no. 8, 081303, [arXiv:1410.7958 \[astro-ph.CO\]](#).
- [29] A. H. Guth, “The Inflationary Universe: A Possible Solution to the Horizon and Flatness Problems”, *Phys.Rev.* **D23** (1981) 347–356.
- [30] F. Lucchin and S. Matarrese, “Power Law Inflation”, *Phys.Rev.* **D32** (1985) 1316.
- [31] A. D. Linde, “Chaotic Inflation”, *Phys.Lett.* **B129** (1983) 177–181.
- [32] L. A. Kofman, “The Origin of matter in the universe: Reheating after inflation”, [arXiv:astro-ph/9605155 \[astro-ph\]](#).
- [33] A. Dolgov and A. D. Linde, “Baryon Asymmetry in Inflationary Universe”, *Phys.Lett.* **B116** (1982) 329.
- [34] A. Albrecht, P. J. Steinhardt, M. S. Turner, and F. Wilczek, “Reheating an Inflationary Universe”, *Phys.Rev.Lett.* **48** (1982) 1437.
- [35] L. Abbott, E. Farhi, and M. B. Wise, “Particle Production in the New Inflationary Cosmology”, *Phys.Lett.* **B117** (1982) 29.
- [36] M. S. Turner, “Coherent Scalar Field Oscillations in an Expanding Universe”, *Phys.Rev.* **D28** (1983) 1243.
- [37] G. N. Felder, J. Garcia-Bellido, P. B. Greene, L. Kofman, A. D. Linde, *et al.*, “Dynamics of symmetry breaking and tachyonic preheating”, *Phys.Rev.Lett.* **87** (2001) 011601, [arXiv:hep-ph/0012142 \[hep-ph\]](#).
- [38] A. R. Liddle, P. Parsons, and J. D. Barrow, “Formalizing the slow roll approximation in inflation”, *Phys. Rev.* **D50** (1994) 7222–7232, [arXiv:astro-ph/9408015 \[astro-ph\]](#).
- [39] W. Buchmüller, V. Domcke, K. Kamada, and K. Schmitz, “The Gravitational Wave Spectrum from Cosmological  $B - L$  Breaking”, *JCAP* **1310** (2013) 003, [arXiv:1305.3392 \[hep-ph\]](#).



- [40] M. Endo, F. Takahashi, and T. T. Yanagida, “Inflaton Decay in Supergravity”, *Phys. Rev.* **D76** (2007) 083509, [arXiv:0706.0986 \[hep-ph\]](#).
- [41] M. Drewes and J. U. Kang, “The Kinematics of Cosmic Reheating”, *Nucl.Phys.* **B875** (2013) 315–350, [arXiv:1305.0267 \[hep-ph\]](#).
- [42] A. Mazumdar and B. Zaldivar, “Quantifying the reheating temperature of the universe”, *Nucl.Phys.* **B886** (2014) 312–327, [arXiv:1310.5143 \[hep-ph\]](#).
- [43] K. Freese, J. A. Frieman, and A. V. Olinto, “Natural inflation with pseudo - Nambu-Goldstone bosons”, *Phys.Rev.Lett.* **65** (1990) 3233–3236.
- [44] F. C. Adams, J. R. Bond, K. Freese, J. A. Frieman, and A. V. Olinto, “Natural inflation: Particle physics models, power law spectra for large scale structure, and constraints from COBE”, *Phys.Rev.* **D47** (1993) 426–455, [arXiv:hep-ph/9207245 \[hep-ph\]](#).
- [45] M. Kawasaki, M. Yamaguchi, and T. Yanagida, “Natural chaotic inflation in supergravity”, *Phys.Rev.Lett.* **85** (2000) 3572–3575, [arXiv:hep-ph/0004243 \[hep-ph\]](#).
- [46] L. Boubekeur and D. Lyth, “Hilltop inflation”, *JCAP* **0507** (2005) 010, [arXiv:hep-ph/0502047 \[hep-ph\]](#).
- [47] E. J. Copeland, A. R. Liddle, D. H. Lyth, E. D. Stewart, and D. Wands, “False vacuum inflation with Einstein gravity”, *Phys.Rev.* **D49** (1994) 6410–6433, [arXiv:astro-ph/9401011 \[astro-ph\]](#).
- [48] A. D. Linde, “Hybrid inflation”, *Phys.Rev.* **D49** (1994) 748–754, [arXiv:astro-ph/9307002 \[astro-ph\]](#).
- [49] F. Brummer, V. Domcke, and V. Sanz, “GUT-scale inflation with sizeable tensor modes”, *JCAP* **08** (2014) 066, [arXiv:1405.4868 \[hep-ph\]](#).
- [50] A. A. Starobinsky, “A New Type of Isotropic Cosmological Models Without Singularity”, *Phys.Lett.* **B91** (1980) 99–102.
- [51] J. Ellis, D. V. Nanopoulos, and K. A. Olive, “No-Scale Supergravity Realization of the Starobinsky Model of Inflation”, *Phys.Rev.Lett.* **111** (2013) no. 12, 111301, [arXiv:1305.1247 \[hep-th\]](#).
- [52] J. Ellis, D. V. Nanopoulos, and K. A. Olive, “Starobinsky-like Inflationary Models as Avatars of No-Scale Supergravity”, *JCAP* **1310** (2013) 009, [arXiv:1307.3537](#).

- [53] W. Buchmuller, V. Domcke, and K. Kamada, “The Starobinsky Model from Superconformal D-Term Inflation”, *Phys.Lett.* **B726** (2013) 467–470, [arXiv:1306.3471 \[hep-th\]](#).
- [54] F. Farakos, A. Kehagias, and A. Riotto, “On the Starobinsky Model of Inflation from Supergravity”, *Nucl.Phys.* **B876** (2013) 187–200, [arXiv:1307.1137](#).
- [55] S. Ferrara, R. Kallosh, and A. Van Proeyen, “On the Supersymmetric Completion of  $R + R^2$  Gravity and Cosmology”, *JHEP* **1311** (2013) 134, [arXiv:1309.4052 \[hep-th\]](#).
- [56] Planck Collaboration, *planck legacy archive*, <http://www.cosmos.esa.int/web/planck/pla>.
- [57] Planck, P. Ade *et al.*, “Planck 2013 results. XXII. Constraints on inflation”, *Astron.Astrophys.* **571** (2014) A22, [arXiv:1303.5082 \[astro-ph.CO\]](#).
- [58] S. Antusch, F. Cefala, D. Nolde, and S. Orani, “False vacuum energy dominated inflation with large  $r$  and the importance of  $\kappa_s$ ”, *JCAP* **1410** (2014) no. 10, 015, [arXiv:1406.1424 \[hep-ph\]](#).
- [59] A. R. Liddle and S. M. Leach, “How long before the end of inflation were observable perturbations produced?”, *Phys.Rev.* **D68** (2003) 103503, [arXiv:astro-ph/0305263 \[astro-ph\]](#).
- [60] Planck, P. Ade *et al.*, “Planck 2015 results. XIII. Cosmological parameters”, [arXiv:1502.01589 \[astro-ph.CO\]](#).
- [61] R. Barbieri and G. Giudice, “Upper Bounds on Supersymmetric Particle Masses”, *Nucl.Phys.* **B306** (1988) 63.
- [62] F. De Bernardis, “Constraints on the reheating temperature of the universe from WMAP-5 and future perspectives”, *Nucl.Phys.Proc.Suppl.* **194** (2009) 39–44.
- [63] K. Ichikawa, M. Kawasaki, and F. Takahashi, “The Oscillation effects on thermalization of the neutrinos in the Universe with low reheating temperature”, *Phys.Rev.* **D72** (2005) 043522, [arXiv:astro-ph/0505395 \[astro-ph\]](#).
- [64] J. Crowder and N. J. Cornish, “Beyond LISA: Exploring future gravitational wave missions”, *Phys.Rev.* **D72** (2005) 083005, [arXiv:gr-qc/0506015 \[gr-qc\]](#).
- [65] S. Kawamura, M. Ando, N. Seto, S. Sato, T. Nakamura, *et al.*, “The Japanese space gravitational wave antenna: DECIGO”, *Class.Quant.Grav.* **28** (2011) 094011.

- [66] K. Nakayama, S. Saito, Y. Suwa, and J. Yokoyama, “Probing reheating temperature of the universe with gravitational wave background”, *JCAP* **0806** (2008) 020, [arXiv:0804.1827 \[astro-ph\]](#).
- [67] J.-O. Gong and E. D. Stewart, “The Density perturbation power spectrum to second order corrections in the slow roll expansion”, *Phys. Lett.* **B510** (2001) 1–9, [arXiv:astro-ph/0101225 \[astro-ph\]](#).
- [68] J. E. Lidsey, A. R. Liddle, E. W. Kolb, E. J. Copeland, T. Barreiro, and M. Abney, “Reconstructing the inflation potential : An overview”, *Rev. Mod. Phys.* **69** (1997) 373–410, [arXiv:astro-ph/9508078 \[astro-ph\]](#).